Caldera formation and progressive batholith construction: Geochronological, petrographic and stratigraphic constraints from the Coxcatlán-Tilzapotla area, Sierra Madre del Sur, Mexico.

Barbara M. Martini *et al.*

GUERRERO
ACADEMIA

REVISTA MEXICANA DE CIENCIAS GEOLÓGICAS

Volumen 30, número 2, agosto 2013

http://www.rmcg.unam.mx

ISSN: 1026-8774

Caldera formation and progressive batholith construction: Geochronological, petrographic and stratigraphic constraints from the Coxcatlán-Tilzapotla area, Sierra Madre del Sur, Mexico

Barbara M. Martiny[1,*], Dante J. Morán-Zenteno[1], Luigi Solari[2], Margarita López-Martínez[3], Shanaka L. de Silva[4], Diana Flores-Huerta[5], Lilibeth Zúñiga-Lagunes[5], and Laura Luna-González[6]

[1] Departamento de Geoquímica, Instituto de Geología, Universidad Nacional Autónoma de México, 04510 México, D.F., Mexico.
[2] Centro de Geociencias, Universidad Nacional Autónoma de México, Campus UNAM Juriquilla, 76230 Querétaro, Mexico.
[3] División de Ciencias de la Tierra, Centro de Investigación Científica y de Educación Superior de Ensenada (CICESE), Carretera Ensenada-Tijuana No. 3918, 22860 Ensenada, Baja California, Mexico.
[4] Department of Geosciences, Oregon State University, Corvallis, OR 97333, U.S.A.
[5] Facultad de Ingeniería, Universidad Nacional Autónoma de México, 04510 México, D.F., Mexico.
[6] Departamento de Geología Regional, Instituto de Geología, Universidad Nacional Autónoma de México, Mexico, D.F., 04510, Mexico.
** martiny@unam.mx*

ABSTRACT

A feature of great interest in the late Eocene-early Oligocene volcanic province of the Sierra Madre del Sur is an elliptical NW-SE oriented dome structure (52 × 30 km) in the Coxcatlán-Tilzapotla region. The elliptical structure encompasses the Tilzapotla collapse caldera, rhyolitic domes, large volumes of ignimbrites, as well as the Buenavista intrusive body, and the Coxcatlán and Chautle plutons located west and east of the structural margin of the caldera, respectively. Previous geochronological studies carried out on the silicic and intermediate magmatic rocks intercalated with pre-caldera tilted terrestrial sediments, as well as the occurrence of an angular unconformity separating fine-grained and coarse-grained beds, constrain uplift in the dome area to the late Eocene (~38-34 Ma). This suggests that doming was related to emplacement of magmas into the crust prior to collapse of the Tilzapotla caldera at 34.3 Ma.

New LA-ICPMS zircon U-Pb and ^{40}Ar-^{39}Ar mineral ages for the key magmatic units combined with field observations, petrographic studies and geochemical analyses reveal the geochronology of magma emplacement and development of the volcano-plutonic complex, and its connection with the dome. Zircon $^{206}Pb/^{238}U$ ages of the Coxcatlán pluton ranging from 39.5 ± 0.6 to 35.2 ± 0.2 Ma suggest that the Coxcatlán pluton was constructed gradually over ~4 m.y. and overlapped in time with the beginning of the development of the Tilzapotla ignimbrite (36.6 ± 0.4 to 33.3 ± 0.5 Ma). Significant overlap of the population density distributions is found indicating temporal continuity of the zircon crystallization record. Zircons from the mafic Chautle pluton (34.37 ± 0.26 Ma) yield the same weighted mean age within uncertainty as zircon from the Tilzapotla ignimbrite. These data are best reconciled with a continuous but incremental assembly of a volcano-plutonic system that climaxed with the caldera collapse and the eruption of the Tilzapotla ignimbrite. The evidence of mafic inputs throughout the history indicates that recharge provided the thermal engine for the prolonged history of the system. Mutual intrusion

Martiny, B.M., Morán-Zenteno, D.J., Solari, L., López-Martínez, M., de Silva, S.L., Flores-Huerta, D., Zúñiga-Lagunes, L., Luna-González, L., 2013, Caldera formation and progressive batholith construction: Geochronological, petrographic and stratigraphic constraints from the Coxcatlán-Tilzapotla area, Sierra Madre del Sur, Mexico: Revista Mexicana de Ciencias Geológicas, v. 30, núm. 2, p. 247-267.

relationships observed between mafic enclaves and granodiorite facies indicate magma mingling within the magma chamber when both host and enclaves were not completely crystallized.

Development of the Coxcatlán-Tilzapotla system resulted in updoming of the surface, extending the "roof" above the melt-rich part of the system in the southeast. The spatial and temporal relationship between the crystal-rich Tilzapotla ignimbrite and the less differentiated Chautle intrusion suggests that mafic magma injection might have disrupted crystal mushes in the chamber, and destabilized the "perched" magma reservoir and thereby triggering the eruption in the southeastern part of the dome.

Key words: volcanic-plutonic connection, ignimbrite, Coxcatlán pluton, Tilzapotla caldera, southern Mexico.

RESUMEN

Un rasgo de mucho interés en la provincia volcánica del Eoceno tardío-Oligoceno temprano de la Sierra Madre del Sur es la estructura dómica de forma elíptica, orientada al NW-SE (52 × 30 km) y ubicada en el área de Coxcatlán-Tilzapotla. La estructura elíptica contiene la caldera de Tilzapotla, domos riolíticos, volúmenes importantes de unidades ignimbríticas, así como el intrusivo de Buenavista y los plutones de Coxcatlán y Chautle, ubicado estos últimos al occidente y al oriente del anillo de la caldera, respectivamente. Los estudios geocronológicos realizados previamente en las rocas magmáticas silícicas y las intermedias intercaladas en sedimentos continentales anteriores a la caldera, así como la presencia de una discordancia angular entre capas de grano fino y grueso, constriñen el tiempo del levantamiento del domo al Eoceno tardío (~38–34 Ma). Lo anterior sugiere que el proceso de formación del domo está relacionado al emplazamiento de magmas en la corteza previo al colapso de la caldera (34.3 Ma).

Nuevas edades de U-Pb por LA-ICPMS en zircones y edades de ^{40}Ar-^{39}Ar en minerales de unidades magmáticas clave, combinadas con observaciones de campo, estudios petrográficos y análisis geoquímicos ponen de manifiesto la geocronología del emplazamiento magmático y el desarrollo del complejo volcánico-plutónico, así como su conexión con el domo. El rango de edades $^{206}Pb/^{238}U$ en circones del plutón de Coxcatlán de 39.5 ± 0.6 a 35.2 ± 0.2 Ma sugiere que el plutón de Coxcatlán se construyó gradualmente durante ~4 m.a. y se traslapa con la historia magmática de la ignimbrita Tilzapotla (36.6 ± 0.4 a 33.3 ± 0.5 Ma). Se observa un traslape significativo en la distribución de edades de las poblaciones que indica una continuidad temporal en el registro de la cristalización de los circones. Los fechamientos de circones del plutón máfico de Chautle arroja una edad igual (34.37 ± 0.26 Ma), dentro del error, a las edades principales de la ignimbrita Tilzapotla. Estos datos se ajustan mejor con un proceso continuo pero creciente de construcción de un sistema volcánico-plutónico que alcanzó su clímax con el colapso de la caldera y la erupción de la ignimbrita Tilzapotla. La evidencia de la inyección de magmas máficos durante este proceso indica que la recarga de magmas proporcionó la energía térmica durante la historia prolongada del sistema magmático. Las relaciones mutuas de intrusión observadas entre los enclaves máficos y la facies de granodiorita indican mezcla inhomogénea (mingling) dentro de la cámara cuando ambas fases no habían alcanzado la cristalización completa.

El desarrollo del sistema Coxcatlán-Tilzapotla resultó en la formación del domo, extendiendo el techo arriba de la zona rica en fundido hacia el sureste. La relación espacial y temporal entre la ignimbrita Tilzapotla, que es rica en cristales, y la intrusión menos diferenciada de Chautle sugiere que la inyección de magmas máficos en la cámara podría haber perturbado las acumulaciones de cristales (mushes) y desestabilizó el reservorio magmático en la parte superior de la corteza causando la erupción en la parte sureste del domo.

Palabras clave: conexión volcánico-plutónica, ignimbrita, plutón de Coxcatlán, caldera de Tilzapotla, sur de México.

INTRODUCTION

There has been considerable debate in recent years about the relationship of large caldera systems and batholiths. The debate has centered on the largest volcanic systems, commonly called "supervolcanic". It is generally agreed that large silicic eruptions can be interpreted in terms of "snapshots" that record conditions in the magma chamber, whereas plutons provide a longer record of magmatic evolution (Bachmann *et al.*, 2007b; Lipman, 2007). However, some view these as separate systems where batholiths represent slow accumulations of silicic magma that never attained eruptibility, while supervolcanic systems represent rapid accumulations of silicic magma that have no plutonic record (Glazner *et al.*, 2004; Coleman *et al.*, 2004, Zimmerer and McIntosh, 2012; Tappa *et al.*, 2011). The alternative

view most recently articulated by the likes of Bachmann *et al.* (2007b), de Silva and Gosnold (2007), Lipman (2007), and Miller (2008) is that large silicic eruptions associated with collapse calderas are intimately related to contemporaneous, consanguineous, co-genetic intrusives, that represent "non-erupted" dominant volumes of the magmatic systems (*e.g.*, Smith, 1979; Lipman, 1984; Elston, 1984). In this view, individual calderas record the development of a pluton and different cycles of activity from that system would mark the progressive or incremental development of that pluton. Collections of spatially and temporally-associated calderas would record the development of a composite batholith at depth. Herein we provide insight into this debate through a study of the Coxcatlán-Tilzapotla region of the Sierra Madre del Sur in Mexico.

The north-central Sierra Madre del Sur (SMS) has been recognized as a site of broad exposures of volcanic and plutonic rocks in the central part of the late Eocene-early Oligocene silicic volcanic province in southern Mexico (Morán-Zenteno *et al.*, 1999). Of particular interest is the Coxcatlán-Tilzapotla area, given its location within a NW-SE oriented elliptical dome structure (52×30 km) that encloses the Tilzapotla caldera, medium-grained plutons, hypabyssal intrusive bodies, rhyolitic domes, and voluminous ignimbrites (Figures 1 and 2). Age and compositional similarities in these broad exposures of volcanic and plutonic rocks suggest a genetic relationship between them, and provide an excellent opportunity for studying the evolution of the magmatic system within the elliptical dome structure and understanding the genetic connection between the volcanic and plutonic realms.

Based on the geochronologic relationships, compositional variations and geochemical characteristics of the voluminous late Eocene-early Oligocene volcanic succes-

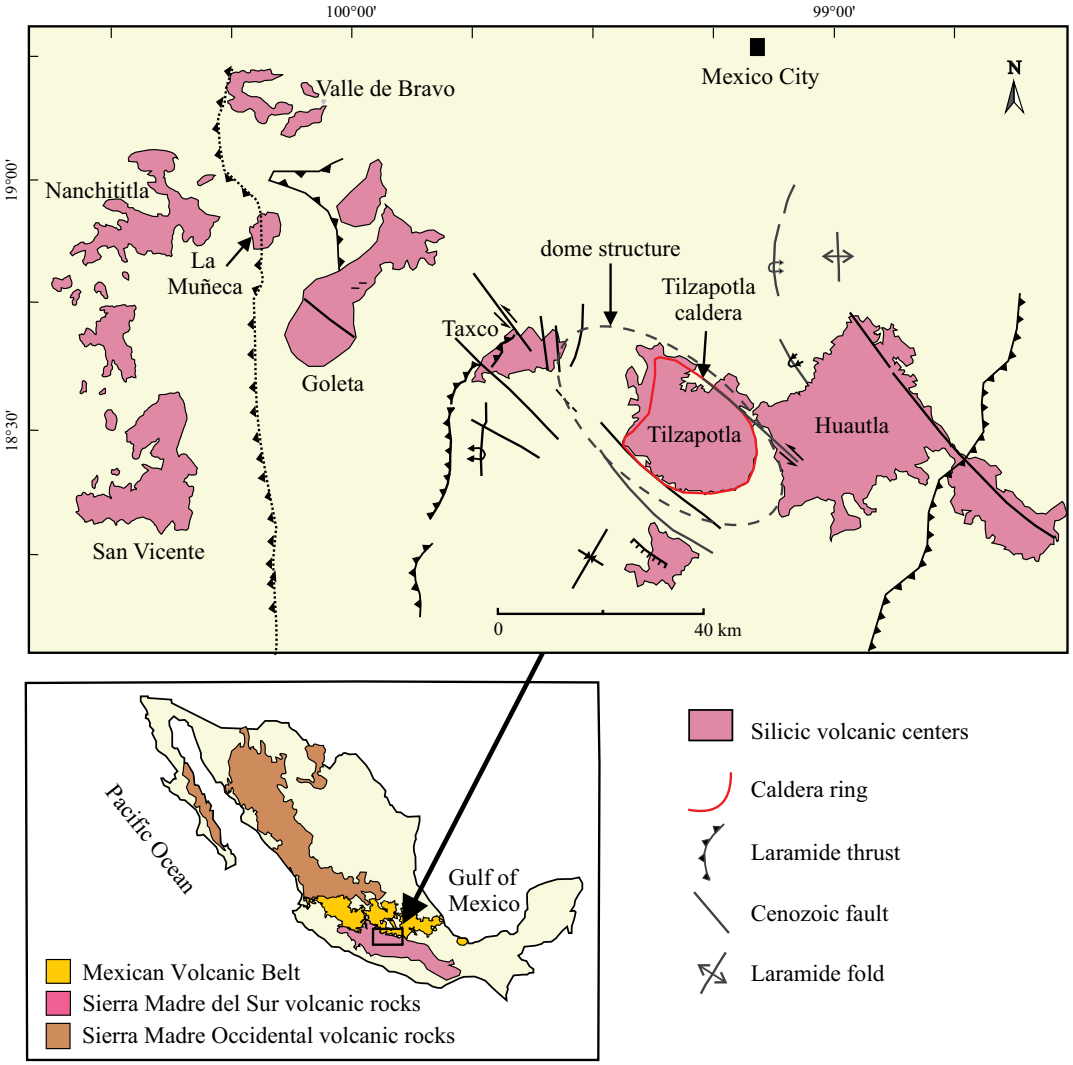

Figure 1. Silicic volcanic centers of the northern Sierra Madre del Sur. Indicated are the elliptical dome structure, Tilzapotla caldera, and near N-trending Laramide structures. Inset indicates the location within Mexico and the large volcanic provinces: Mexican Volcanic Belt (Miocene-Recent), Sierra Madre del Sur (late Eocene-early Oligocene), and Sierra Madre Occidental (Oligocene-early Miocene). Modified from Morán-Zenteno *et al.* (2004).

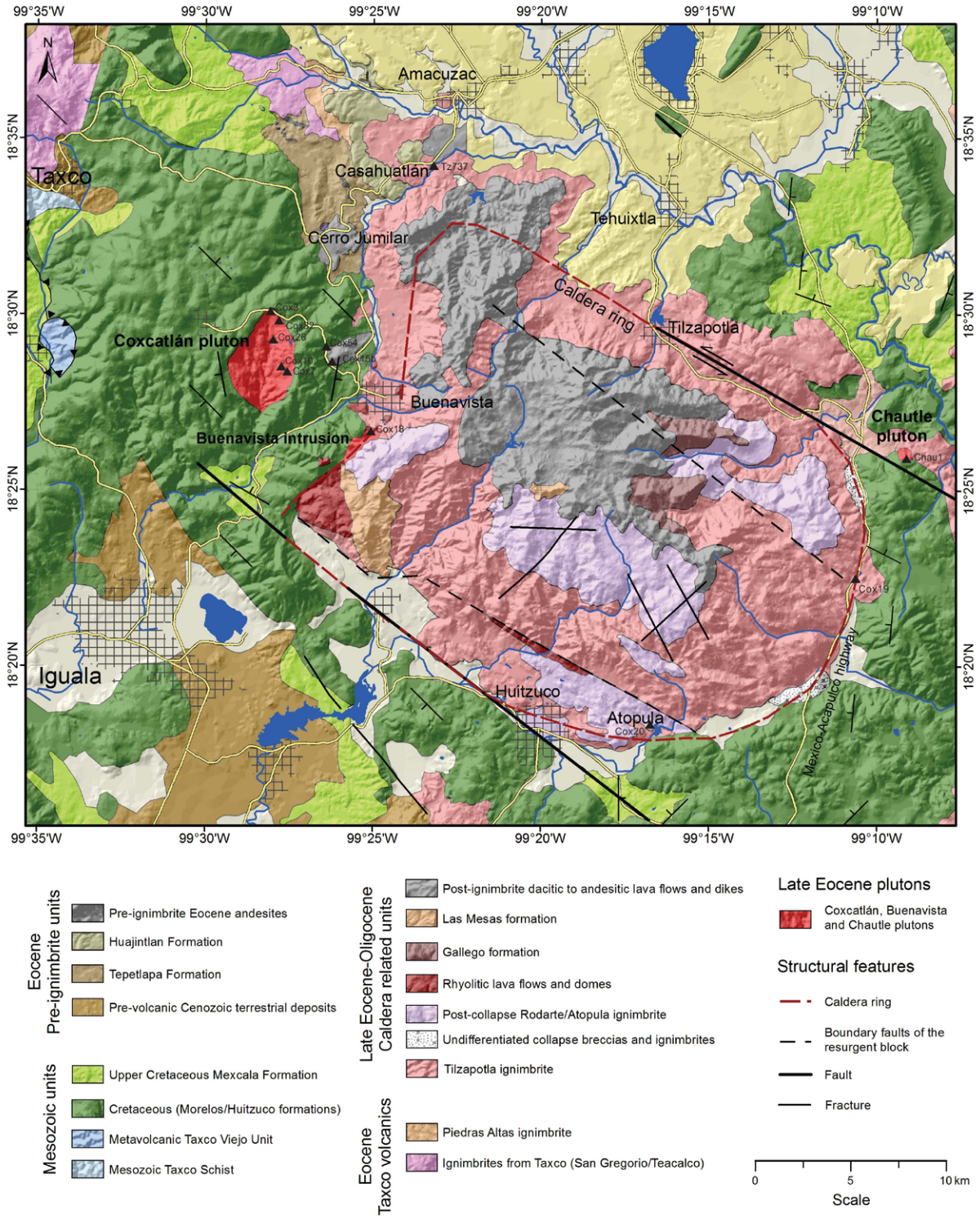

Figure 2. Geological map of the Coxcatlán-Tilzapotla area. Indicated are the Coxcatlán and Chautle plutons, the Buenavista intrusion, the Tilzapotla caldera ring structure, and related tectonic features.

sions, Mori *et al.* (2012) interpreted the origin of the silicic centers in terms of the gradual thermomechanical maturation of the crust due to a sustained mantle power input during the Eocene. This group of silicic centers displays volume-time patterns similar to those documented and summarized by de Silva *et al.* (2006) and de Silva and Gosnold (2007) and are thus interpreted as the sequence of events and conditions that trigger the formation of ignimbrite flare-ups.

Regional geological and geochronological studies were carried out previously by our group near the ellipti-

cal dome structure in the silicic magmatic rocks, the tilted pre-volcanic continental sediments and intercalated volcanic rocks, as well as the underlying deformed Cretaceous marine sedimentary rocks. Results suggested uplifting in this region during the late Eocene (~38–34 Ma) and a doming process related to the emplacement of magma into the upper crust prior to extrusion of the Tilzapotla ignimbrite at 34.3 Ma, which is associated with the caldera collapse (Morán-Zenteno *et al.*, 2004; Morán-Zenteno *et al.*, 2007). Dome construction was initially interpreted by Morán-Zenteno *et al.* (2004) as the expression of the tumescence stage in the development of the Tilzapotla caldera; however, results presented here indicate a more complex scenario.

Earlier studies in the Coxcatlán-Tilzapotla sector focused mainly on the volcanic rocks and pre-volcanic continental sedimentary rocks, whereas plutonic and hypabyssal intrusive rocks exposed along and outside of the Tilzapotla caldera ring, the structural margin of the caldera, have received less attention (Figure 2).

The present study is based on new LA-ICP-MS zircon U-Pb and Ar-Ar mineral ages for several of the different magmatic facies within the elliptical dome structure, with emphasis on the plutonic and hypabyssal rocks (Coxcatlán and Chautle plutons, Buenavista intrusion) in order to identify intrusive rocks that are contemporaneous with the Tilzapotla ignimbrite and caldera collapse, and gain insight on plutonic-ignimbrite connections. We include description of the petrography of different magmatic facies of the Coxcatlán pluton, including magmatic enclaves, the Tilzapotla ignimbrite and related units. In addition we document the temporal evolution of magma emplacement within the elliptical dome. Particular attention was focused on the development of the elliptical dome structure and its possible relationship to the progressive construction of a batholith at depth under the Coxcatlán-Tilzapotla region.

GEOLOGICAL SETTING AND STRATIGRAPHY OF THE COXCATLÁN-TILZAPOTLA AREA

The Tilzapotla caldera area is part of the subduction related magmatic record in the SMS that extends over a broad region in southern Mexico and became extinct between the early Oligocene and early Miocene (Schaaf *et al.*, 1995; Morán-Zenteno *et al.*, 1999). Magmatic activity in the Coxcatlán-Tilzapotla sector formed part of a major episode of late Eocene to early Oligocene explosive silicic activity preceded by pulses of andesitic and mafic volcanism in the north-central SMS. Silicic volcanism produced voluminous ignimbrites, collapse caldera structures, rhyolitic domes, pyroclastic dikes, hypabyssal intrusive bodies and intermediate to silicic lavas between Nanchititla and Huautla (Figure 1). General rejuvenation in the region led to the partial exhumation of most of the Paleogene silicic centers and the exposure of feeding conduits and plutonic counterparts. After the Paleocene volcanism died out at ~28 Ma, arc volcanism reinitiated at 20 Ma in a more northern position in the Trans Mexican Volcanic Belt (Ferrari *et al.*, 2012).

Silicic volcanism of the Coxcatlán-Tilzapotla area covers folded Cretaceous marine and sedimentary units that include calcareous and clastic beds of the Morelos/Huitzuco and Mexcala formations (Fries, 1960); it also overlies Eocene terrestrial deposits with intermediate and mafic dikes and lavas intercalated in the sequence (Balsas Group) (Fries, 1960; Morán-Zenteno *et al.*, 2007) (Figure 2).

The structural dome associated with the Tilzapotla-Coxcatlán magmatic system is a NW-SE oriented elliptical structure with a long axis of 52 km and a short axis of 30 km (Figure 1). The 30×20 km collapse caldera structure is contained in the southeastern part of the dome, whereas the Coxcatlán pluton is located in the northwestern part. Compared with pre-volcanic ~N-S folds characteristic of the Late Cretaceous - Paleocene shortening in the region (Laramide), the Coxcatlán-Tilzapotla dome clearly displays a different orientation of its long axis. The effects of this structural interference are expressed by the northward and southward plunging of the small-scale Laramide folds on the northern and southern flanks of the dome, respectively (Figures 1 and 3). Timing of the dome formation has been constrained by an angular unconformity and a significant facies change between two Eocene terrestrial successions exposed outside the northwestern edge of the structural dome. The lower and upper successions are separated by ignimbrites dated by K-Ar in sanidine at 38.5 ± 0.7 Ma and 35.1 ± 0.4 Ma (Morán-Zenteno *et al.*, 2007). Tilting of the lower succession, as well as a coarsening-upward tendency observed in the upper part of the lower succession, is indicative of rejuvenation of the landscape due to uplift of the Coxcatlán-Tilzapotla dome structure. The occurrence of ignimbrites as old as 38.5 Ma between the two successions and tilting of the upper succession away from the dome structure indicate that uplift had already initiated at least 38 m.y. ago and continued until ~34 Ma, when the Tilzapotla caldera collapsed.

Volcanic stratigraphy

Ignimbrites associated with caldera collapse, post-caldera ignimbrites and rhyolitic domes in the Tilzapotla area were erupted from 35.5 to ~33 Ma (Morán-Zenteno *et al.*, 2004). The pre-silicic volcanic record is represented by low volume andesitic to mafic lavas and dikes intercalated with and intruding the terrestrial deposits of the Balsas Group (Fries, 1960; de Cserna and Fries, 1981), which include the Tepetlapa and Huanjintlán formations cropping out northwest of the dome structure (Morán-Zenteno *et al.*, 2007). Intercalated with the Balsas Group and separating the Tepetlapa and Huanjintlán formations are ignimbrite flows dated at 38.5 ± 0.7 and 35.1 ± 0.4 Ma; the earlier ignimbrite has the same age within uncertainty as basal sanidine-rich

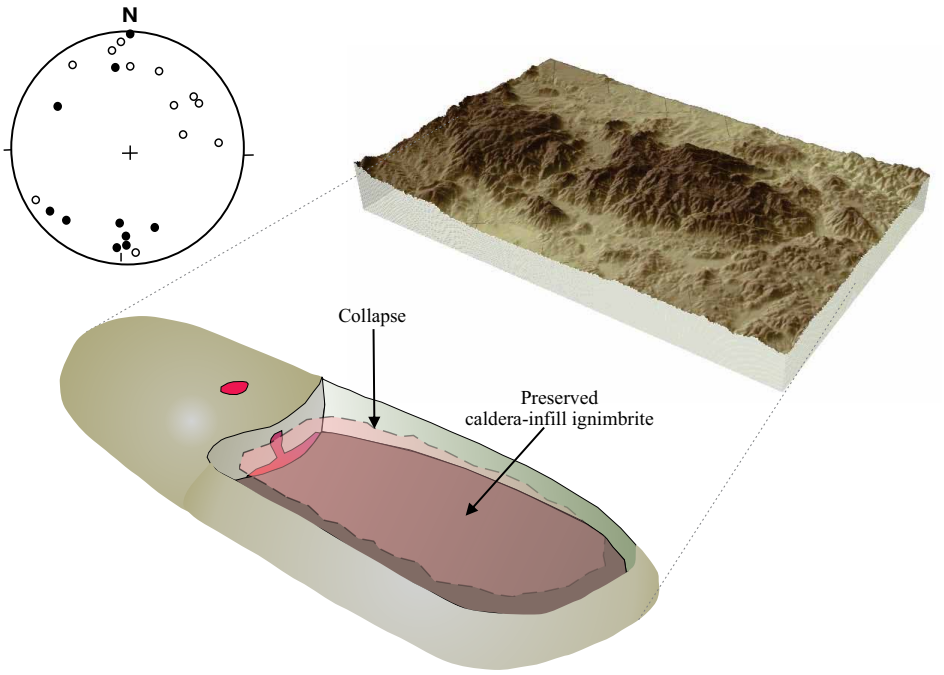

Figure 3. Digital elevation model of the elliptical dome structure, with cartoon showing the collapse caldera in the southeast sector of the dome. Stereonet diagram plots small scale Laramide fold axes north (white circles) and south (black circles) of the dome. Modified from Morán-Zenteno *et al.* (2004, 2007).

ignimbrites of the neighboring Taxco volcanic center, suggesting that the two flows are related (Morán-Zenteno *et al.*, 2007). The upper dacitic to andesitic lava flows and dikes in the caldera area span from 33 to 32 Ma and are related to resurgence that produced uplift of the central block of the caldera infill (Figure 2) (Morán-Zenteno *et al.*, 2007).

The Tilzapotla ignimbrite (Figure 4a), which is interpreted as the pyroclastic unit related to the collapse, varies in exposed thickness from at least 600 m in the caldera interior to 50–150 m of preserved ignimbrite sections outside the caldera (Morán-Zenteno *et al.*, 2004). The intra-caldera ignimbrite succession is formed by at least five flows that display differences in the relative abundances of lithic and pumice components. Phenocryst abundance in pumice fragments varies typically from 25% to 35%, although in basal units of the northern extra-caldera facies the abundance is less than 5%. The main phenocryst phases in order of abundance are quartz, plagioclase, sanidine and biotite. Traces of altered hornblende are also present. The groundmass of the ignimbrites is generally devitrified and is composed of microcrystalline quartz and feldspar. The caldera ring on the north and south sides coincides with NW-SE trending faults that record post-collapse lateral displacement (Figure 2). The ignimbrite facies near the ring has relatively high abundance of limestone lithics and some sections display collapse megabreccia. We therefore interpret the "ring" as the structural margin of the caldera.

Post-collapse silicic units include the Rodarte and Atopula ignimbrites that overlie debris flows and conglomerate deposits derived from the Tilzapotla ignimbrite. The Rodarte ignimbrite contains large crystal-poor pumice fragments, whereas the Atopula unit displays crystal-rich (30–40%) pumice fragments. Relative phenocryst phase abundances are similar to the Tilzapotla ignimbrite, with quartz dominating over plagioclase and sanidine. In the central area of the caldera these units are overlain by the Gallego formation, a ~50 m succession of vitrophyres interpreted as having been formed from densely welded crystal poor ash flows. A series of rhyolitic domes with characteristic flow structure are distributed along the western segment of the caldera ring.

The post-ignimbrite volcanic record is represented by a succession of hornblende dacite to pyroxene-bearing andesitic lava flows and feeding dikes, up to 200 m thick, that are distributed in the central and northwestern sectors of the caldera. The succession includes the dacitic to andesitic El Salto formation and the andesitic Rodeo formation (Morán-Zenteno *et al.*, 2004). Differential erosion of the caldera and uplift related to the resurgence led to inverted relief, so that the top of the caldera infill ignimbrites and lavas are now at higher elevations than the surrounding Mesozoic calcareous rocks (Morán-Zenteno *et al.*, 2004).

Plutonic record

The intrusive record is represented by three plutons located outside of, but relatively close to, the caldera struc-

Figure 4. Field photographs from the Coxcatlán-Tilzapotla area. a) Tilzapotla ignimbrite containing slightly flattened pumice; b) Mafic magmatic enclave (MME) hosted in the Coxcatlán pluton. Rounded form suggests plastic deformation within a fluid host. Double magmatic enclave (darker enclave within lighter enclave) suggests mingling of magmas of different compositions. Note reaction rim in contact zone between the MME and Coxcatlán pluton; c) Felsic magmatic enclave in the Coxcatlán pluton; d) Lobate form of MME in the light gray colored Coxcatlán granodiorite; e) Aligned belt of MME observed in the southern part of the Coxcatlán pluton; f) Double magmatic enclave in the Coxcatlán pluton; g) Felsic and mafic enclaves side by side; h) Magmatic enclave swarm in the southern part of the Coxcatlán pluton.

tural margin and within the structural dome containing the Tilzapotla caldera. Their position within the dome and the spatial and temporal proximity to the Tilzapotla caldera strongly suggest that they belong to the same magmatic system that produced the caldera. The largest exposure, located west of the structural margin, corresponds to the Coxcatlán pluton (Figure 2), which represents a shallow apophysis of the deeper silicic reservoir in the uncollapsed part of the dome that has been exposed by drainage incision. The other two plutons are represented by small exposures located along the structural margin southwest of Buenavista (Buenavista intrusion) and east of the structural margin (Chautle pluton). The characteristics of the plutonic exposures in the vicinity of the Tilzapotla caldera were poorly known and only brief mention has been made of the intrusive rocks in a local publication and a technical report (Ontiveros-Tarango, 1973; Carrizales-Aguilar, 1997), in several works focused on different geological features of the north-central sector of the SMS (Fries 1960, 1966), and in more recent works that include radiometric age data (Meza-Figueroa *et al.*, 2003; Morán-Zenteno *et al.*, 2004). The present work is part of an ongoing study to examine the intrusive exposures, and represents the first study of the field, petrographic and geochemical characteristics of the plutons, with focus on the largest of the intrusive bodies, the Coxcatlán pluton.

The Coxcatlán pluton, emplaced in Cretaceous limestone, is exposed over an area of about 18 km^2 and comprises at least two apparently coeval facies. Thin sections of 41 samples from the Coxcatlán pluton were studied in a petrographic microscope in order to characterize mineralogical and textural features. Modal analyses were carried out mainly to determine the amounts of quartz, K-feldspar and plagioclase present. Field observations indicate that most of the exposed pluton is a light gray colored, medium-grained rock speckled with variable amounts of dark minerals. In some parts of the pluton, crystals of plagioclase and alkali feldspar noticeably larger than the surrounding medium-grained minerals are common. These megacrysts are mostly <1 cm, but can reach up to 2 cm or more. Modal mineral analyses indicate that the Coxcatlán pluton plots mainly as monzogranite-granodiorite on a Streckeisen (1976) QAP diagram, with some samples extending into the quartz monzonite field (Figure 5); for simplicity, in this work the dominant facies of the Coxcatlán pluton is generally referred to below as a granodiorite. In this facies, biotite is ubiquitous (up to ~10%), minor hornblende (<2%) is often but not always present, and scarce pyroxene (up to 1%) and sometimes two pyroxenes were identified in a small number of samples. Titanite has not been observed. The granodiorite displays textural, mineralogical and slight geochemical variations. A finer-grained variety, exposed in the interior part of the pluton, is somewhat lighter in color compared to the dominant facies due to the smaller content of ferromagnesian minerals (<5% biotite). Light colored felsic magmatic enclaves (see below) enclosed in the granodiorite could testify to an additional subsequent pulse of silicic magma. Xenoliths, rarely observed in the pluton, measure from 9 to 15 cm in length and have lithologies similar to those of the country rock.

The second facies is represented by pyroxene-bearing magmatic enclaves, which are an important feature of the granodiorite. Mafic magmatic enclaves (MME) are ubiquitous and are finer-grained and darker than the host rock (Figure 4b, 4d, 4e, 4f, 4h); scarce felsic enclaves have been observed in the southern part of the pluton (Figure 4c). Most enclaves have ellipsoidal or rounded shapes, although some have irregular or lobate forms (Figure 4d); these forms suggest plastic deformation within a still fluid host. Contacts between the magmatic enclaves and the host rocks can be sharp with chilled margins or diffuse. Magmatic enclaves are usually <10 cm in length, but can reach up to 20 cm or more. Aligned belts of MME suggest dismembered dikes emplaced in a still fluid host rock (Figure 4e). Mafic magmatic enclaves contain up to 10% quartz but typically less, plagioclase > potassic feldspar, and usually plot as quartz monzodiorites and monzodiorites in the QAP Streckeisen diagram (yellow circles in Figure 5). MME have a much higher content of ferromagnesian minerals with respect to the granodiorite. They contain abundant biotite (usually 10–20%, reaching up to 25%) and pyroxene (usually <10%, but up to 15%); minor hornblende (generally <3%) can be present, but is observed as a reaction product of pyroxene in the transitional contact zone with the host granitoid. In a few enclaves elongate biotite grains show moderate to strong alignment, reflecting magmatic flow. Large plagioclase and alkali feldspar megacrysts are often observed in the MME and could have been transferred from the host granitoid when both magmas were still partially molten (Vernon,

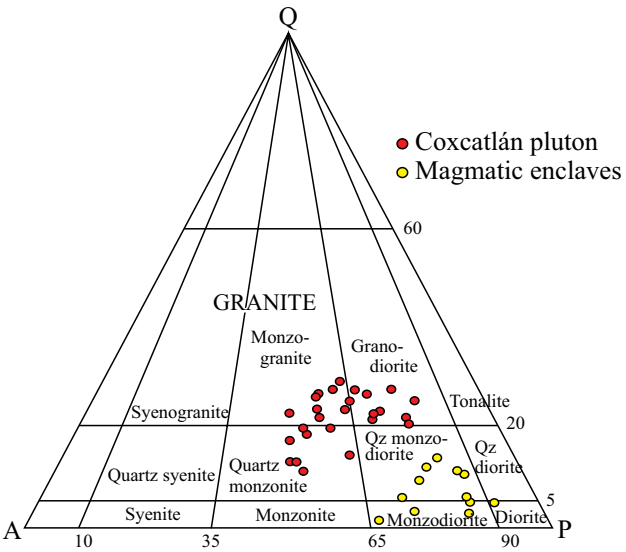

Figure 5. QAP diagram for the plutonic rocks (Streckeisen, 1976). Red circles: Coxcatlán pluton; yellow circles: mafic magmatic enclaves hosted in the Coxcatlán pluton.

1986; Barbarin, 1990). Double magmatic enclaves (enclave within enclave) are frequently observed (Figure 4f). The presence of rounded to elongate enclaves, lobate contacts, double magmatic enclaves, and mafic and felsic enclaves side by side (Figure 4g) are features that suggest mingling (Vernon *et al.*, 1988) in which pulses of magma of different compositions were injected into the host granodiorite. Mafic magmatic swarms are observed in the southern sector of the Coxcatlán pluton (Figure 4h).

We have not observed any composite dikes in the area. Occasional thin aplite veins seven to eight cm wide are observed different parts of the Coxcatlán pluton, and a small aplite mass of approximately 40 cm is exposed in the northern sector of the pluton, along the highway to the northwest of the town of Coxcatlán. The aplitic rock is fine-grained and is constituted mainly by quartz and feldspar intergrowth in a graphic texture, with small amounts (~1%) of biotite and oxides.

Recent widening of the highway at the northern edge of the Coxcatlán pluton has exposed small pegmatite lenses and a contact aureole between the granodiorite and Cretaceous limestone; yellow-brown garnet crystals in this zone measure 1–3 mm, but can reach 1.5 cm in diameter. X-ray diffraction in whole rock and clay-sized (<2 μm) fractions identified calcite, wollastonite, spessartite, vesuvianite, and smectite in the contact aureole. XRD analyses were preformed with a Shimadzu XRD-6000, equipped with a monochromator, using Cu radiation.

The Buenavista intrusion is a porphyritic subvolcanic body exposed in an area of approximately 2×0.5 km at the southern limits of the town of Buenavista de Cuéllar, and is limited to the east by ignimbrites and to the west by Mesozoic limestone, where it is associated with a Fe skarn deposit. It consists of phenocrysts of altered plagioclase crystals with disequilibrium features and embayed anhedral quartz grains, with scarce biotite in a fine granular silicified groundmass. Meza-Figueroa *et al.* (2003) report $^{40}Ar/^{39}Ar$ plateau ages of 35.5 ± 0.6 Ma and 34.7 ± 0.6 Ma for two different experiments on biotite of the Buenavista intrusion.

The Chautle pluton is a small intrusive body emplaced in Cretaceous limestone beds at a distance of ~3 km east of the caldera ring. It is a dark gray, fine- to medium-grained rock that contains plagioclase of variable size that includes fine- to medium-grained crystals as well as large crystals showing disequilibrium features such as sieve texture, oscillatory zoning, and resorbed margins. The Chautle pluton contains two pyroxenes (15–20%) with minor amounts of biotite (<5%), and has a dioritic composition, which is significantly more mafic than the dominant facies of the Coxcatlán pluton.

GEOCHEMISTRY

Major elements were determined by fused disk X-ray fluorescence spectrometry at the Laboratorio Universitario de Geoquímica Isotópica (LUGIS) of the Universidad Nacional Autónoma de México (UNAM), using a Siemens SRS-3000 spectrometer, following procedures outlined by Lozano and Bernal (2005).

Whole rock major element analysis of volcanic units of the Tilzapotla caldera show a dacitic composition for the collapse-related Tilzapotla ignimbrite (~67–69 wt% SiO_2); post-collapse/pre-resurgence products have dacitic to rhyolitic compositions (~67–74 wt% SiO_2), and lava flows related to resurgence (34.4 to 32.8 Ma) have andesitic to dacitic compositions (57–65 wt% SiO_2) (Morán-Zenteno *et al.*, 2004). Late stage volcanic rocks exposed between Buenavista and Coxcatlán were analyzed in this study; a hypabyssal unit (sample Cox15b) displays an andesitic composition with SiO_2 of ~57 wt% and a dacitic vitrophyre (sample Cox54) contains ~65% SiO_2 (Table 1).

Geochemical analyses carried out on a group of intrusive rocks within the Coxcatlán-Tilzapotla elliptical structure display significant compositional variations in the late Eocene-early Oligocene plutonic record (Table 1). West of the caldera ring, the dominant facies of the Coxcatlán pluton ranges in composition from granite to granodiorite (~71 to 69 wt% SiO_2 (Cox26 and Cox7, respectively), but magmatic enclaves in the granitoids are generally much more mafic, and present a dioritic composition (SiO_2 = ~53 wt%, Cox32). East of the caldera ring, the Chautle pluton (Chau1) is also more mafic than the dominant facies of the Coxcatlán pluton, with SiO_2 of ~55 wt%.

In a geochemical study of the late Eocene-early Oligocene volcanic centers of the north-central SMS, Mori *et al.* (2012) suggest that the evolution of andesitic to

Table 1. Whole rock major element analyses of magmatic rocks in the Coxcatlán-Tilzapotla area.

Sample	Rock	Location		SiO_2	TiO_2	Al_2O_3	Fe_2O_3	MnO	MgO	CaO	Na_2O	K_2O	P_2O_5	LOI	Total
Cox26	Coxcatlán pluton	99°27.98'	18°29.28'	70.97	0.32	14.78	2.44	0.03	0.78	1.78	3.36	4.38	0.14	0.76	99.75
Cox7	Coxcatlán pluton	99°27.61'	18°28.30'	68.95	0.52	15.15	4.15	0.07	1.27	2.87	3.34	3.52	0.14	0.35	100.35
Cox32	MME in Coxcatlán pluton	99°27.82'	18°29.78'	53.20	1.11	17.15	9.32	0.15	4.36	7.62	3.26	2.52	0.20	0.84	99.73
Chau1	diorite	99°09.11'	18°25.95'	55.63	1.02	17.31	8.23	0.13	5.13	7.42	2.88	1.55	0.19	0.43	99.91
Cox54	vitrophyre	99°26.39'	18°28.99'	65.49	0.48	15.58	3.26	0.07	1.34	3.76	3.03	3.33	0.19	3.63	100.16
Cox15b	andesite	99°26.19'	18°28.63'	56.50	1.11	18.47	7.28	0.11	3.68	6.74	3.35	1.42	0.34	0.39	99.38

rhyolitic rocks associated with the Tilzapotla caldera was dominated by low-pressure fractional crystallization of pyroxene and plagioclase assemblages, with assimilation of Rb-enriched middle-upper crustal rocks to produce the dacitic and rhyolitic compositions. This interpretation was based on a coherent decrease of MgO, CaO, Al_2O_3 and Sr concentrations with increasing silica contents, a negative correlation between Eu/Eu* and the differentiation index, and similar La/Yb and Sm/Yb ratios throughout the suite, which precludes the crystallization of garnet, a high pressure mineral with high partitions coefficients for heavy rare earth elements such as Sm and Yb. This is confirmed by high $^{143}Nd/^{144}Nd$ ratios, low $^{87}Sr/^{86}Sr$ ratios, and a negative correlation between $^{143}Nd/^{144}Nd$ and SiO_2.

COMPARATIVE ANALYSIS OF THE GEOCHRONOLOGICAL DATA FROM THE PLUTONIC AND VOLCANIC ROCKS IN THE COXCATLÁN-TILZAPOTLA REGION

Geochronological dating was performed on distinct magmatic units not only to attempt to better constrain the evolution of magmas within the elliptical dome structure in the Coxcatlán-Tilzapotla caldera area, but also to explore pluton growth and the duration of the magmatic system prior to eruption. We present $^{40}Ar/^{39}Ar$ mineral dating and U-Pb LA-ICPMS dating of zircon, in a number of instances from the same sample, of several intrusive bodies and extrusive units (Table 2).

$^{40}Ar/^{39}Ar$ geochronology

Analytical methods

Seven mineral separates were prepared from six whole rock samples collected in the Coxcatlán-Tilzapotla area. Four of the mineral separates were obtained from three samples collected in different parts of the Coxcatlán pluton: biotite-bearing samples Cox3 (biotite) and Cox10 (biotite and alkali feldspar), and biotite-poor sample Cox26 (alkali feldspar). Other samples dated are the Chautle diorite (plagioclase, sample Chau1), an intermediate volcanic rock (plagioclase, sample Cox15b), and the Atopula ignimbrite (sanidine, sample Cox20).

The samples were prepared at the Mineral Separation Laboratory of the Departamento de Geología at the Centro de Investigación Científica y de Educación Superior de Ensenada (CICESE), Ensenada, Baja California, Mexico. The basic sample preparation consisted of crushing and sieving, then rinsing with distilled water followed by 98% acetone. The rock fragments were dried overnight at ~60 °C. The minerals were then concentrated by Frantz magnetic separator to insure >99% purity. Samples were

Table 2. Summary of ^{40}Ar-^{39}Ar and U-Pb geochronological data.

Sample	Location	Mineral	Unit	Preferred Ar-Ar ages and K-Ar ages (Ma)		Apparent $^{206}Pb/^{238}U$ zircon age (Ma)
Cox3	99°28.03' 18°30.12'	biotite	Coxcatlán pluton	36.28 ± 0.23	t_p	
Cox10	99°27.68' 18°28.48'	alkali feldspar	Coxcatlán pluton	35.84 ± 0.37	t_c	35.75 ± 0.28
Cox10	99°27.68' 18°28.48'	biotite	Coxcatlán pluton	35.76 ± 0.13	t_c	
Cox26	99°27.98' 18°29.28'	alkali feldspar	Coxcatlán pluton	36.97 ± 0.12	t_p	36.01 ± 0.36
Chau1	99°09.11' 18°25.95'	plagioclase	Chautle diorite	34.54 ± 0.55	t_p	34.37 ± 0.26
Cox20	99°16.87' 18°18.16'	sanidine	Atopula ignimbrite	33.74 ± 0.29	t_c	33.18 ± 0.28
Cox15b	99°26.19' 18°28.63'	plagioclase	Hypabyssal andesite	30.77 ± 0.90	t_p	
Cox32	99°27.82' 18°29.78'		MME in Coxcatlán pluton			36.75 ± 0.26
Cox18	99°25.10' 18°26.59'	biotite[a]	Buenavista intrusion	1st exp 35.5 ± 0.6[a] 2nd exp 34.7 ± 0.6[a]	t_p[a]	35.17 ± 0.18
Cox19	99°10.64' 18°22.62'	sanidine[b]	Tilzapotla ignimbrite	34.26 ± 0.09[b]	one-step[b]	34.32 ± 0.26
Tz737	99°23.27' 18°34.13'	biotite[c]	Tilzapotla ignimbrite	34.3 ± 1.5[c]	K-Ar[c]	34.23 ± 0.20

All age determinations from present work unless otherwise indicated. t_p = plateau age; t_c = isochron age; one-step = one-step fusion experiment on single crystals, a: Sample ABC07 (Meza-Figueroa *et al*., 2003) collected from a location near Cox18; b: Sample Sol 2 (Morán-Zenteno *et al.*, 2004) from same location as Cox19; c: Sample Tz145-01 (Morán-Zenteno *et al.*, 2004) collected from a location near Tz737.

selected by handpicking under a binocular microscope from fractions ranging in size <710 to >350 μm for samples Cox10 and Cox 20. Samples Cox3, Cox15b, Cox26 and Chau1 range in size from <350 to >250 μm. As irradiation monitor, aliquots of sanidine FCT 2 (28.201 ± 0.046 Ma; Kuiper *et al.*, 2008) were irradiated alongside the samples. The samples and monitor were irradiated with Cd-liner at the University of McMaster (Hamilton, Ontario) in the U-enriched research reactor receiving a dose of 30 MW. The ^{40}Ar-^{39}Ar experiments were conducted at the Geochronology Laboratory at CICESE using a Coherent Ar-ion Innova 370 laser extraction system on-line with a VG5400 mass spectrometer. The irradiation monitors were fused in one step. All the samples were step-heated and additionally for sanidine Cox20 four one-step fusion experiments were performed. All the argon experiments were preceded by a blank measurement, with the five argon isotopes measured. Upon blank subtraction, the argon isotopes were corrected for radioactive decay, mass discrimination, calcium, potassium and chlorine neutron induced interference reactions. In processing the data, the decay constants and isotopic composition recommended by Steiger and Jäger (1977) were used. Equations given by York *et al.* (2004) were used in all straight-line calculations.

Results

^{40}Ar-^{39}Ar results are summarized in Table 2 with full ^{40}Ar-^{39}Ar data of all the experiments in the electronic appendix A1, and details of each sample analyzed presented in appendix A2. Figures with age spectra and the ^{36}Ar/^{40}Ar versus ^{39}Ar/^{40}Ar correlation diagrams for each sample are presented in Figure 6. Note that all errors are reported at 1σ level. The errors in the integrated, plateau and isochron age include the uncertainty in the irradiation parameter *J*. Additionally, for the plateau and isochron ages, the goodness of fit was included in the age uncertainty whenever the MSWD exceeded 1. The integrated ages were calculated adding the fractions of the step-heating experiments. Plateau ages were calculated with the weighted mean of three or more consecutive fractions, which were in agreement within 1σ errors excluding the uncertainty in *J*.

In general, the ^{40}Ar-^{39}Ar and K-Ar age data are consistent with geologic relations and magmatic stratigraphy. Where available, biotite and alkali feldspar ages are concordant, suggesting that inherited-Ar is not a problem at this age range (*e.g.*, Hora *et al.*, 2010). The Coxcatlán pluton yields the oldest ages, ranging from 36.97 ± 0.12 to 35.76 ± 0.13 Ma. At the 2σ level these ages are still discordant suggesting a protracted cooling history in a body of significant volume. The Tilzapotla ignimbrite yields generally younger K-Ar and ^{40}Ar-^{39}Ar ages of 34.3 ± 1.5 and 34.26 ± 0.09 Ma, respectively, although the K-Ar age is relatively imprecise and is concordant within error with the younger Coxcatlán age. The ages of the subordinate units of the Chautle diorite, Buenavista intrusion, and Atopula ignimbrite are consistent with them representing post-caldera activity (Morán-Zenteno *et al.*, 2004) and a general eastward younging of the magmatic system.

U-Pb LA-ICPMS zircon geochronology

Analytical methods

The eight samples selected for zircon geochronology were crushed and standard techniques such as Wilfley separation and heavy liquids were used for mineral separation. Zircon concentrates were observed under a binocular microscope and approximately 100 grains were selected from each sample, taking care to include all the morphological, shape and color variations. The selected grains were mounted in epoxy resin, ground by hand to expose half of the crystals, and imaged by cathodoluminescence using an ELM 3R luminoscope (Marshall, 1988).

LA-ICP-MS U-Pb analyses were performed at the Laboratorio de Estudios Isotópicos (LEI), Centro de Geociencias, UNAM, using a Resolution M050 excimer laser workstation coupled with a Thermo Xseries quadrupole ICPMS. The Plešovice standard zircon (*ca.* 337 Ma; Sláma *et al.*, 2008) was used as bracketing standard. All the analyses were performed employing a spot of 32 μm in diameter and a fluence of *ca.* 6 J/cm^2. A 1-sigma external reproducibility of 0.6% (^{206}Pb/^{238}U ratio), 0.95% (^{207}Pb/^{206}Pb ratio) and 1.1% (^{208}Pb/^{232}Th ratio) was measured on such standard zircon, and quadratically propagated to the unknown measured ratios, to take into account the natural standard inhomogeneity. Further details of the analytical procedures are given in Solari *et al.* (2010). The obtained raw data were reduced, and errors propagated, using internally developed software (Solari and Tanner, 2011). When needed, the common Pb contribution was corrected using the algebraic method of Andersen (2002), provided that the ^{204}Pb signal is generally swamped by the ^{204}Hg interference and cannot be correctly evaluated by the current instrumentation. The obtained data were screened and filtered, following a discordance criteria (all the analyses which yielded more than 30% and less than -5% discordance were considered unreliable and thus discarded), and then an error criteria on isotopic ratios (all the analyses which corrected isotopic ratios yielded more than 5% 1 sigma error were discarded). Finally, further screening was performed observing rare earth element (REE) patterns, as well as some trace-element contents, such as P and La. The presence of analyses with high values (*e.g.*, >1500 ppm P and >30 ppm La) strongly suggests that an apatite inclusion was hit during analysis, and were thus discarded. U and Th content were screened cautiously, because the higher their content, the greater the probability of crystal damage from radioactive decay, and thus of possible Pb loss. In due case, those analyses were also discarded.

The concordia plots, deconvolution calculations, and age-error calculations were completed using Isoplot v. 3.7 (Ludwig, 2008). Especially useful for the Paleogene ages

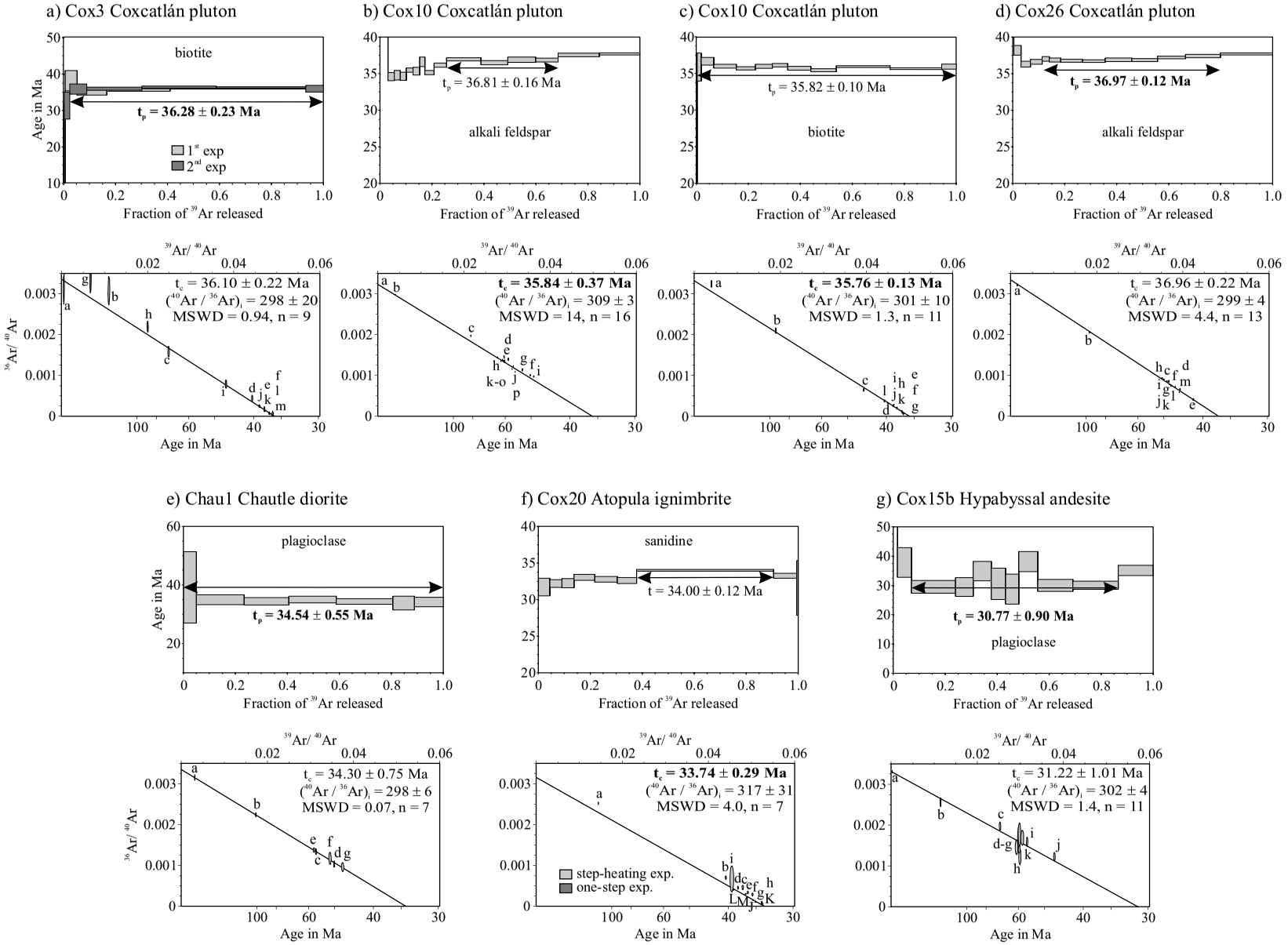

Figure 6. ^{39}Ar/^{40}Ar age spectra and isochron diagrams for igneous rocks within the elliptical structural dome in the Coxcatlán-Tilzapotla area. a) Coxcatlán pluton sample Cox3; b) and c) Coxcatlán pluton sample Cox10; d) Coxcatlán pluton sample Cox26. e) Chautle diorite sample Chau1. f) Atopula ignimbrite sample Cox20. g) Hypabyssal andesite sample Cox15b. Preferred age in bold letters. All errors are reported at 1σ level.

presented below are the mean $^{206}Pb/^{238}U$ ages, given that the measurement of ^{207}Pb is problematic in those young zircons, and the consequent uncertainty in the $^{207}Pb/^{206}Pb$ ratio is not a good indicator of geologically meaningful discordances. It is also common to observe scattering in the mean $^{206}Pb/^{238}U$ ages, which yield MSWD (mean square of weighted deviates) values that are largely greater than one, an indication that the possibility of mixed age-populations exists. To try and recognize the different age components in those samples that showed an initial MSWD generally above 3, we used the deconvolution method implemented in Isoplot and based on the Sambridge and Compston (1994) mixture modeling method. Once the mixture components were recognized, their mean $^{206}Pb/^{238}U$ ages were plotted together with errors and recalculated MSWD in Figure 7. This figure includes U-Pb concordia plots (first column); deconvolution diagrams with frequency curves (red curves) or population density plots (PDP) and, for comparative purposes, $^{40}Ar/^{39}Ar$ ages where available (second column); and mean age diagrams (on the right side of Figure 7).

Results

Details of analyzed zircons from the samples are given in appendices A3 and A4, and a summary of the apparent ages is given in Table 2. Details of the age data for each sample are in narrative form in appendix A2. Descriptions of most samples dated by this method are given above in the sections on "Geological setting and stratigraphy of the Coxcatlán-Tilzapotla area" and Appendix A2.

Complex populations are revealed in population density plots or PDPs (Figure 7). Individual zircon ages in deconvolution plots (Figure 7, second column) reveal almost continuous distributions, but show slight breaks that suggest different pulses of zircon crystallization. This was confirmed by the application of the unmixing algorithm (Sambridge and Compston, 1994), by which two or three different populations with distinct weighted mean ages were obtained for each sample.

Inherited ages and core-rim age variations in single zircons

It is now well established that volcanic rocks often record a significant pre-magmatic history of inherited or xenocrystic "basement" zircons. Additionally, "antecrysts", zircons from an earlier confocal magmatic episode, are also common. The dominant population however, should be "autocrysts", zircons that grew in the erupted magma (*e.g.*, Miller *et al.*, 2007, Folkes *et al.*, 2011). The youngest zircon populations seen in the PDPs (Figure 7) correspond to these "autocrysts", whereas the older populations correspond to "antecrysts".

Cathodoluminescence imaging revealed cores in some of the zircon grains, and oscillatory growth zoning was frequently observed. Cox 10 and 26 and Chau1 have a significant number of grains ranging in age from Precambrian to middle Eocene that are consistent with the age of basement units in the region (*e.g.*, Elías-Herrera *et al.*, 2000; Talavera-Mendoza *et al.*, 2005, 2007), or that can be explained by assimilation of sedimentary or metasedimentary crustal units.

It is interesting to note that inherited zircon grains in the Coxcatlán-Tilzapotla samples are often of a different size and shape when compared to the main zircon population. The characteristics of the main zircon populations in the eight samples studied display certain variations (Table 3). In general, the late Eocene zircon autocrysts studied are colorless to pale yellow, have elongated prismatic shapes, measure from ~130 to 340 μm in length, and have aspect ratios of 2 to 4, with some exceptions; for example, many of the zircon grains are noticeably larger in Tilzapotla ignimbrite sample Tz737 (Table 3). In contrast, in Coxcatlán pluton sample Cox10 two small (~100 μm), dark stubby inherited zircons yielded a slightly discordant age of 526 Ma and a concordant age of 65 Ma, and an unusually large, dark zircon has a core age of 167 Ma.

The larger size of the cores and growth zones in some of the zircon grains allowed exploring age variations between cores and rims. Analyses in two zircon grains of the Coxcatlán pluton yielded core-rim age pairs of 167 and 164 Ma, and 92 and 35.6 Ma, respectively (Table A3, sample Cox10). Additional core-rim analyses in the samples yielded late Eocene age pairs that are interpreted as different pulses of the magma system that were injected into the magma chamber during different stages of development. Seven core-rim age pairs are indicated in the deconvolution plots of Figure 7, in which each pair has the same color error bar. Core-rim age variations in the seven pairs range from 1.6 to 3.4 m.y. Core ages correspond to one of the earlier mean age groups obtained and are interpreted as antecrysts. Rim ages correspond to the younger mean age group defined by autocrysts.

We turn our attention now to the autocrysts. These

Figure 7 (following two pages). U-Pb zircon ages of samples dated by LA-ICPMS. In the first column on the left are U-Pb Tera-Wasserberg concordia diagrams, in the second column are deconvolution diagrams, and on the right are mean age diagrams. In the deconvolution diagrams, U-Pb zircon ages between 32 and 40 Ma are illustrated by diamonds with associated error bars; numbers on the vertical axis refer to the number of zircon analyses; red lines are frequency curves or population density plots (PDP), vertical black lines indicate the mean $^{206}Pb/^{238}U$ ages with error (gray shaded areas), and the green dashed lines indicate $^{39}Ar/^{40}Ar$ ages. Concordia diagrams, frequency curves, and errors were calculated using Isoplot 3.7 (Ludwig, 2008). Deconvolution diagrams were calculated using Isoplot, based on the unmixing model method developed by Sambridge and Compston (1994). Data-point error ellipses on concordia diagrams, and age error bars for mean ages on the deconvolution diagrams and mean age figures are 2σ from the $^{206}Pb/^{238}U$ weighted mean age. a) Coxcatlán pluton, Cox10; b) Coxcatlán pluton, Cox26; c) Mafic magmatic enclave, Cox32, embedded in the Coxcatlán pluton; d) Buenavista intrusion, Cox18; e) Chautle diorite, Chau1; f) Tilzapotla ignimbrite – Acapulco highway, Cox19; g) Tilzapotla ignimbrite – Cerro El Jumilar, Tz737; h) Atopula ignimbrite, Cox20.

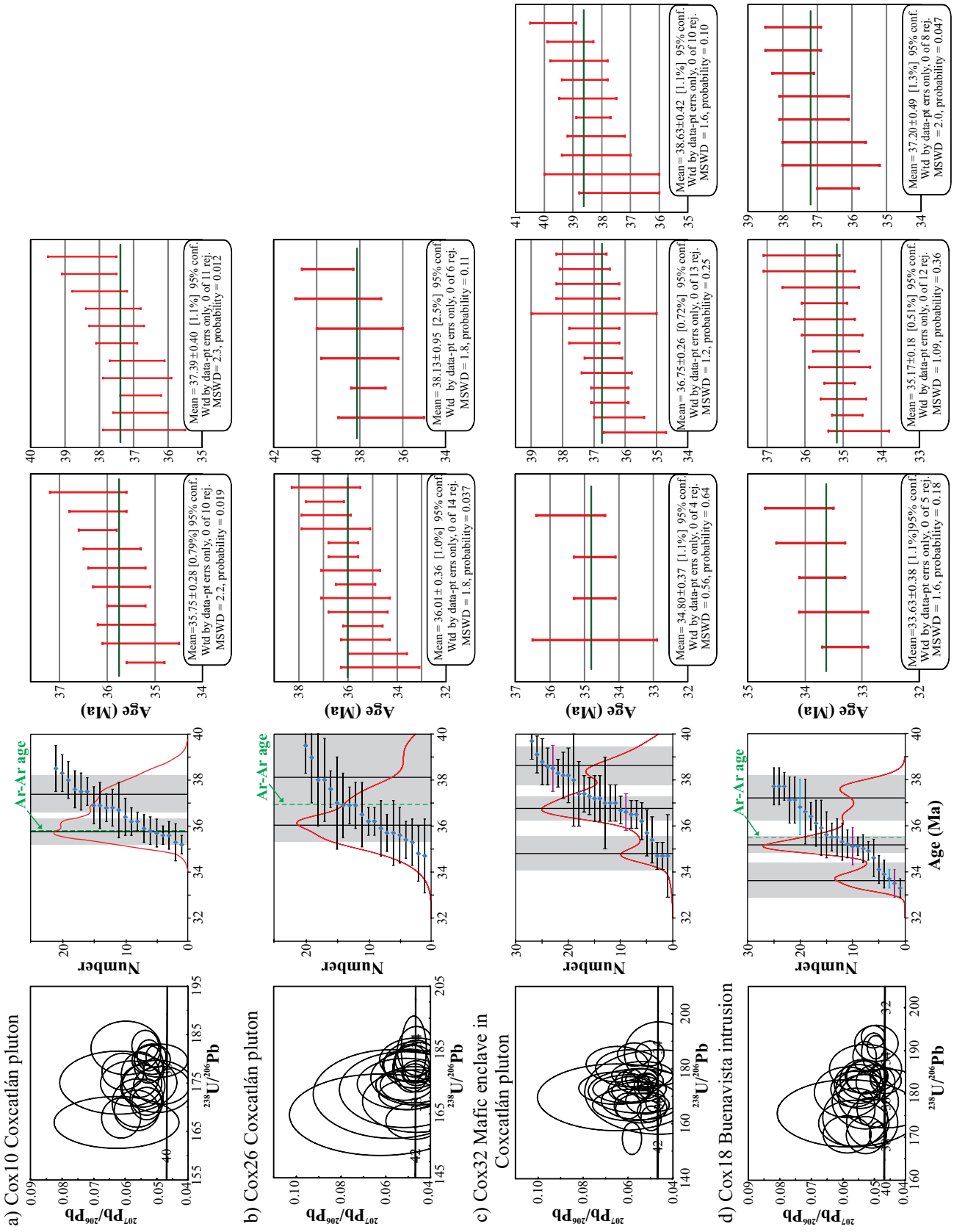
a) Cox10 Coxcatlán pluton
b) Cox26 Coxcatlán pluton
c) Cox32 Mafic enclave in Coxcatlán pluton
d) Cox18 Buenavista intrusion
$^{207}Pb/^{206}Pb$
$^{238}U/^{206}Pb$
Ar-Ar age
Number
Age (Ma)
Mean=35.75±0.28 [0.79%] 95% conf. Wtd by data-pt errs only, 0 of 10 rej. MSWD = 2.2, probability = 0.019
Mean = 37.39±0.40 [1.1%] 95% conf. Wtd by data-pt errs only, 0 of 11 rej. MSWD= 2.3, probability = 0.012
Mean = 36.01± 0.36 [1.0%] 95% conf. Wtd by data-pt errs only, 0 of 14 rej. MSWD = 1.8, probability = 0.037
Mean = 38.13±0.95 [2.5%] 95% conf. Wtd by data-pt errs only, 0 of 6 rej. MSWD = 1.8, probability = 0.11
Mean= 34.80±0.37 [1.1%] 95% conf. Wtd by data-pt errs only, 0 of 4 rej. MSWD = 0.56, probability = 0.64
Mean= 36.75±0.26 [0.72%] 95% conf. Wtd by data-pt errs only, 0 of 13 rej. MSWD = 1.2, probability = 0.25
Mean=33.63±0.38 [1.1%]95% conf. Wtd by data-pt errs only, 0 of 5 rej. MSWD = 1.6, probability = 0.18
Mean = 35.17±0.18 [0.51%] 95% conf. Wtd by data-pt errs only, 0 of 12 rej. MSWD = 1.09, probability = 0.36
Mean = 38.63±0.42 [1.1%] 95% conf. Wtd by data-pt errs only, 0 of 10 rej. MSWD = 1.6, probability = 0.10
Mean = 37.20±0.49 [1.3%] 95% conf. Wtd by data-pt errs only, 0 of 8 rej. MSWD = 2.0, probability = 0.047

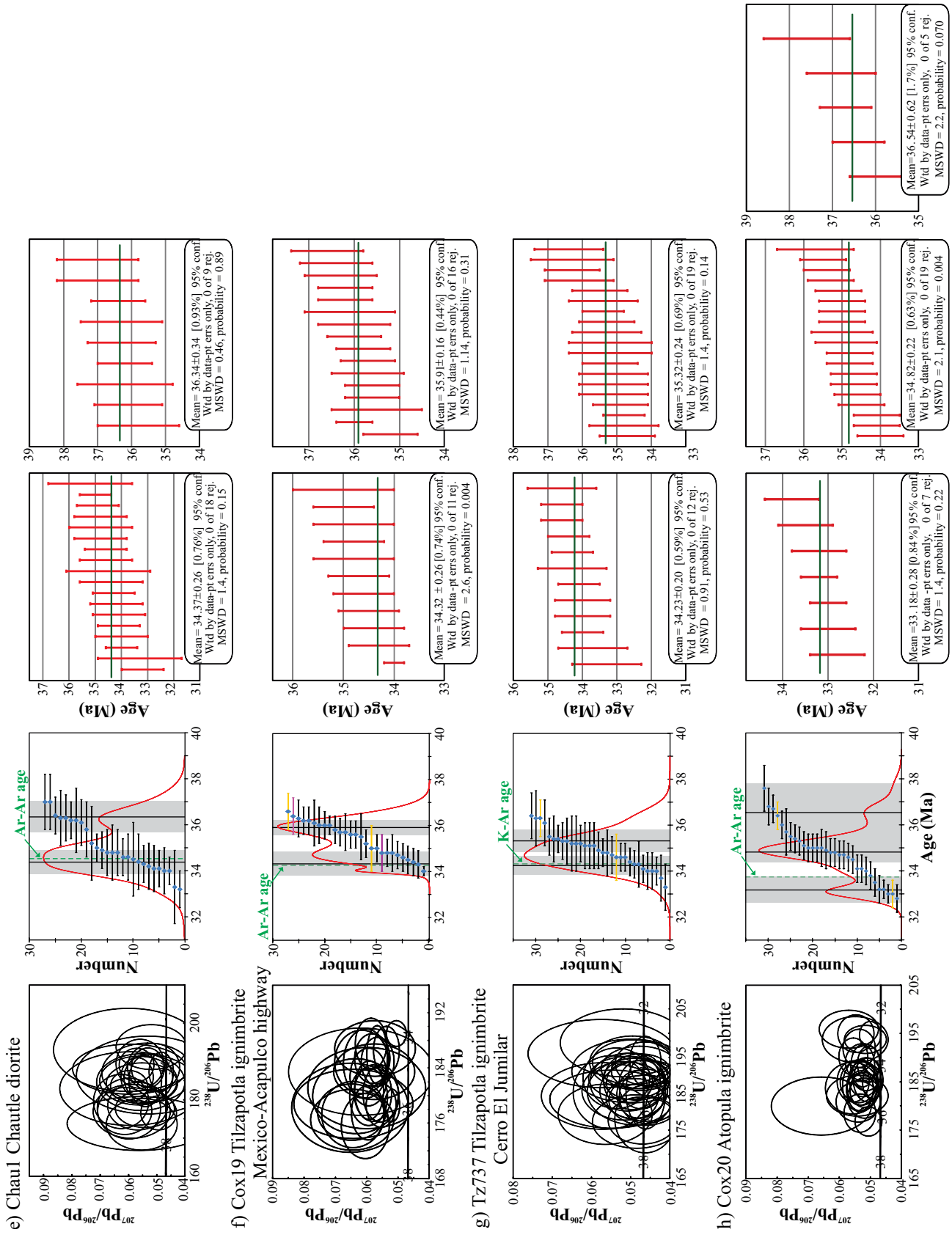
e) Chaul Chautle diorite
f) Cox19 Tilzapotla ignimbrite Mexico-Acapulco highway
g) Tz737 Tilzapotla ignimbrite Cerro El Jumilar
h) Cox20 Atopula ignimbrite
Ar-Ar age
K-Ar age
Number
Age (Ma)
$^{207}Pb/^{206}Pb$
$^{238}U/^{206}Pb$
Mean= 34.37±0.26 [0.76%] 95% conf
Wtd by data-pt errs only, 0 of 18 rej.
MSWD = 1.4, probability = 0.15
Mean= 36.34±0.34 [0.93%] 95% conf
Wtd by data-pt errs only, 0 of 9 rej.
MSWD = 0.46, probability = 0.89
Mean = 34.32 ± 0.26 [0.74%] 95% conf.
Wtd by data-pt errs only, 0 of 11 rej.
MSWD = 2.6, probability = 0.004
Mean= 35.91±0.16 [0.44%] 95% conf
Wtd by data-pt errs only, 0 of 16 rej.
MSWD = 1.14, probability = 0.31
Mean= 34.23±0.20 [0.59%] 95% conf
Wtd by data-pt errs only, 0 of 12 rej.
MSWD = 0.91, probability = 0.53
Mean= 35.32±0.24 [0.69%] 95% conf
Wtd by data-pt errs only, 0 of 19 rej.
MSWD = 1.4, probability = 0.14
Mean =33. 18±0.28 [0.84%] 95% conf
Wtd by data -pt errs only, 0 of 7 rej.
MSWD= 1.4, probability = 0.22
Mean= 34.82±0.22 [0.63%] 95% conf
Wtd by data-pt errs only, 0 of 19 rej.
MSWD = 2.1, probability = 0.004
Mean=36. 54±0.62 [1.7%] 95% conf.
Wtd by data-pt errs only, 0 of 5 rej.
MSWD = 2.2, probability = 0.070

record the most recent episode of magmatism and hold the keys to understanding the development of the magmatic system.

DISCUSSION

The record of zircon autocrysts

Miller *et al.* (2007) regard the lower age trend of zircon arrays as autocrysts representing the best approximation of the crystallization age, as the last zircon growth or complete solidification of the pluton, assuming that Pb loss can be discounted. For the geochronological data obtained in the Coxcatlán-Tilzapotla area, the youngest mean ages in the deconvolution plots of Figure 7 are thus interpreted as the mean apparent age of the pluton or magma batch. The interpretation of the these ages as mean apparent magmatic ages is confirmed by the $^{40}Ar/^{39}Ar$ mineral ages obtained, which are indistinguishable within uncertainty from the apparent age of the sample (Figure 7, Table 2).

Weighted mean autocryst ages for the two samples of the Coxcatlán pluton are significantly older than those from the two samples of Tilzapotla ignimbrite. However, in detail the significance of this statistical discordance is offset by some interesting overlap in the individual. For instance, individual zircons from the Tilzapotla ignimbrite define a range in age from 36.6 ± 0.4 to 33.3 ± 0.5 Ma (1σ), while Coxcatlán pluton zircons range in age from 39.5 ± 0.6 to 35.2 ± 0.2 Ma. The autocryst populations of the two units show significant overlap in the PDPs, rim ages of Coxcatlán pluton autocrysts are younger or overlap with core ages of Tilzapotla zircons, and some individual Coxcatlán zircons that have ages concordant with Tilzapotla ignimbrite zircons. We cannot reasonably attribute any of the overlap to Pb loss in the Coxcatlán pluton based on coherence of the data on the Tera-Wasserberg concordia plots. Thus, despite the statistical discordance of the weighted mean ages, we interpret these records to indicate significant overlap of zircon crystallization in the Coxcatlán pluton and the Tilzapotla ignimbrite.

The Buenavista intrusion, on the west caldera rim and east of the Coxcatlán pluton, displays a wide range of zircon ages from 37.7 to 33.3 Ma. A major peak at ~35 Ma is defined in the PDP (Figure 7d), and yields a weighted mean age within error of the $^{40}Ar/^{39}Ar$ biotite plateau ages of 35.5 and 34.7 Ma obtained by Meza-Figueroa *et al.* (2003). Compared to the Coxcatlán pluton, zircon crystallization in the Buenavista intrusion began and ended later, but took place over a similar time period (~4 m.y.).

In two samples (MME sample Cox32 and Buenavista intrusion sample Cox18), the youngest mean ages are represented by a small group of data with error bars that display little overlap with the main zircon population and are somewhat younger than the $^{40}Ar/^{39}Ar$ ages (Figure 7). Again we cannot reject these as due to Pb loss as these appear coherent on the Tera-Wasserberg plots. They must represent real zircon crystallization ages and attest to discordance between U-Pb zircon ages and ^{40}Ar-^{39}Ar biotite ages in Cox 18 (no Ar-Ar age is available for Cox 32). We note that the ^{40}Ar-^{39}Ar biotite age came from a different but closely located sample to Cox 18, that biotite can be open to Ar and K exchange during alteration, and that a skarn deposit is in this area.

Ages for Cox 32 for the mafic enclave in the Coxcatlán pluton show significant overlap with the pluton data. The Buenavista intrusion sample Cox 18 also shows significant overlap. However, a significantly younger autocryst popu-

Table 3. Samples dated by U-Pb zircon analysis: multiple analyses in single zircons and characteristics of analyzed grains.

Sample	Unit	Core and rim ages (Ma) in single zircons	Zircon color	Zircon size[a] (µm)	Aspect ratio[b]
Cox10	Coxcatlán pluton	167 and 164; 92 and 35.6; 39.9 and 35.6	colorless to pale yellow	200-250, up to 340	2 to 3.5, up to 4.5
Cox26	Coxcatlán pluton		colorless	125-270, up to 340	2–3, up to 3.7
Cox32	Magmatic enclave in Coxcatlán pluton	38.5 and 36.6	colorless to pale yellow	165-280	2.6–3.4
Cox18	Buenavista intrusion	36.8 and 33.7; 35.1 and 33.5	colorless to pale yellow	160-260, up to 600	2.5–4
Chau1	Chautle diorite		colorless to very pale yellow	130-260, up to 400	1.3–2.3
Cox19	Tilzapotla ignimbrite	36.6 and 35.0 36.4 and 34.8	colorless to pale yellow	130-330	2.5–4
Tx737	Tilzapotla ignimbrite	36.3 and 34.6	colorless to pale yellow	200-535	3–5.7
Cox20	Atopula ignimbrite	36.4 and 33.0	colorless to pale yellow	150-260, up to 400	2.5–3.4

a: Average and maximum zircon size; b: Average and maximum zircon aspect ratio (length to width ratio).

lation appears to be recorded in the Chautle diorite (37.0 to 33.2 Ma) and the Atopula ignimbrite (37.6 to 32.8 Ma).

Age patterns in the Coxcatlán-Tilzapotla area

Significant overlap in all the zircon populations suggests continuous zircon crystallization in the Coxcatlán-Tilzpotla system as distinct batches of magma evolved over an approximately 6 m.y. period to build a significant volcano-plutonic complex. During this time, some of the complexity in the zircon populations could have been produced by recharge events, as evidenced by the Chautle, MME, and the young andesite. Hot magma intruding into a cooler, incompletely crystallized magma body preserved as supra-solidus crystal mush could result in changing the conditions of zircon saturation sufficiently to cause significant complexity. We are unable to resolve such events categorically but note the possibility of this for further investigation.

A spatial trend of younger zircon ages is recorded to the east, not only in the Tilzapotla ignimbrite, which is the most voluminous volcanic unit and is associated with caldera collapse in the eastern sector of the dome, but also in the Chautle diorite and Atopula ignimbrite (Figure 7). Ar-Ar geochronological data for these units are also younger. We interpret this to suggest a generally eastward migrating magmatic focus. It is of interest to note the U-Pb zircon apparent ages obtained for the Tilzapotla ignimbrite and Chautle diorite are the same within error, indicating a temporal relationship between the two units and suggesting a shared magmatic history (Figures 7e, 7f, 7g), in which the emplacement of mafic batches similar to and coeval with the Chautle diorite into the magma chamber could have triggered ignimbrite eruption and caldera collapse.

Compared to the Tilzapotla ignimbrite, post-collapse ignimbrites (*i.e.*, Atopula unit along the southern caldera limit) display a nearly continuous range in the zircon age data of ~4 m.y., starting at ~37 Ma and extending to a younger array at ~33 Ma, indicating the arrival of new batches of silicic magma into the chamber. ^{40}Ar-^{39}Ar ages of the dacitic to andesitic lava flow units associated with the resurgence of the central block of the caldera floor and infill range from 33 to 32 Ma (Morán-Zenteno *et al.*, 2004).

The southeastward younging trend of the zircon ages reveals that batholith construction underneath the Coxcatlán-Tilzapotla dome progressed from west to east as pulses arrived in series into the upper crust. Individual pulses may have been emplaced sufficiently closely in time and space to have shared zircon crystallization histories, at least in part, as evidenced by overlap of rim and core ages in Coxcatlán pluton and Tilzapotla ignimbrite, respectively. The younging trend in the magmatic activity is illustrated in Figure 8. In the first stage, beginning at ~39.5 Ma, magma batches were emplaced in the western part and crystallized over a period of ~4 m.y. probably sustained by mafic

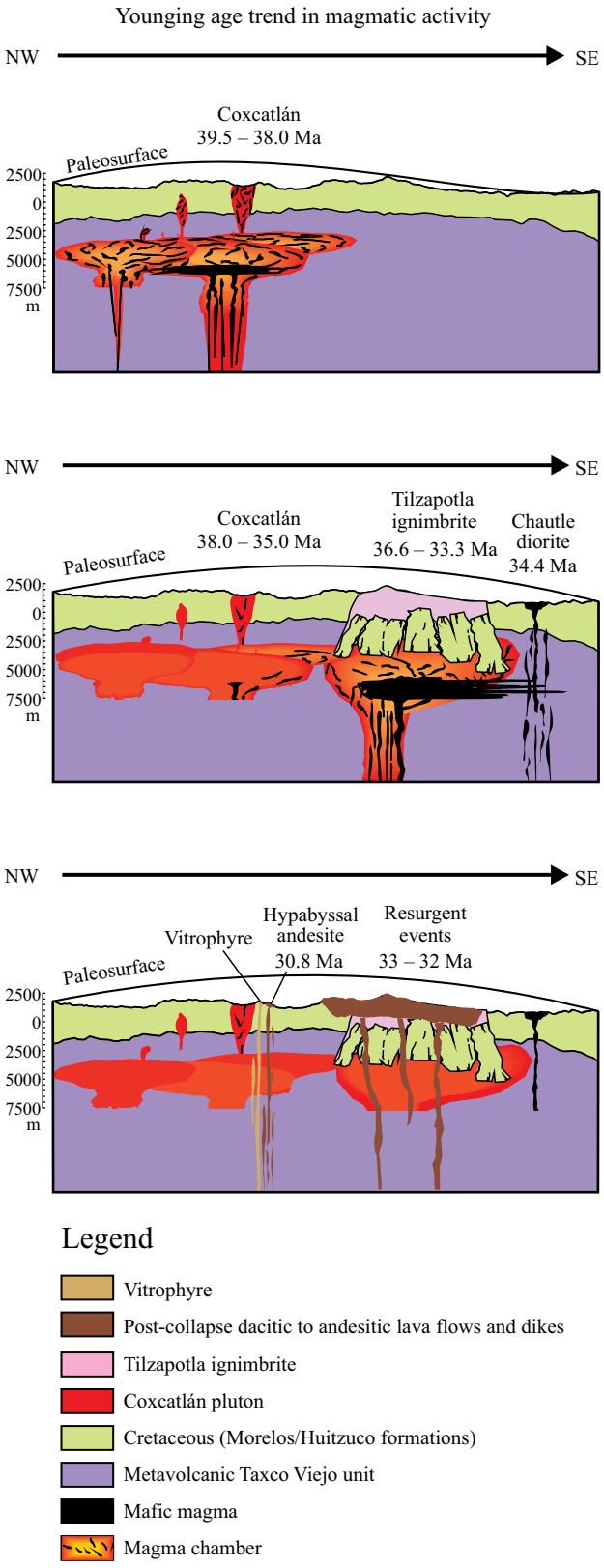

Figure 8. Sequence of sketches of the structural dome in the Coxcatlán-Tilzapotla area, illustrating the main magmatic episodes and the southeastward-younging age trend in magmatic activity. See text for explanation.

recharge. This produced an initial doming deformation in this sector. As the magmatic focus moved eastward, the most significant thermal anomaly developed from 36.6 to 33.3 Ma, leading to the construction of a significant eruptible magma volume that extended the doming effect to the east. This doming in response to development of a major silicic magmatic system is consistent with classic geological observations of pre-caldera tumescence (*e.g.*, Smith and Bailey, 1968) and recent thermomechanical models of caldera systems (Gregg *et al.*, 2012). Continued intrusion of mafic magmas is evidenced by the Chautle diorite approximately concordant with eruption of the Tilzapotla ignimbrite and caldera collapse. Finally (~33–31 Ma) a series of silicic and intermediate injections of magma produced caldera resurgence and minor volcanic episodes outside the caldera.

Batholith construction in the Coxcatlán-Tilzapotla area

Recent advances of in situ U-Pb zircon dating of volcanic and plutonic rocks have shown that granitoid plutons (*e.g.*, McNulty *et al.*, 1996, 2000; Coleman *et al.* 2004; Glazner *et al.*, 2004; Matzel *et al.*, 2006; Lipman, 2007; Miller *et al.*, 2007; Tappa *et al.*, 2011) as well as the volcanic products of silicic magma systems (*e.g.*, Schmitt *et al.*, 2003; Reid, 2003; Bachmann *et al.*, 2007a, 2007c; Folkes *et al.*, 2011) record a multistage history of numerous pulses of magmas that accumulate over time and cannibalize their progenitors. We clearly see evidence for this in the Coxcatlán-Tilzapotla elliptical dome structure. We believe that the record here is one of incremental but continuous assembly of batholith from numerous pulses of magma. The nearly continuous age range observed for all samples suggest an approximately 6 m.y. period for the development of the system. This is consistent with, for example, Cretaceous batholiths in the western United States that have a duration of >5 m.y. for Mt. Stuart (Matzel *et al.*, 2006) and >8 m.y. for Tuolumne (Coleman *et al.*, 2004).

The Coxcatlán pluton seems to represent an apophysis of a deep-seated plutonic complex, and displays textural and mineralogical diversity in addition to features that we interpret as key aspects in the understanding of the magmatic system evolution. It is located in a segment of the structural dome where no significant volcanic conduits have been identified and where there is no caldera development. The overlapping age distributions (39.5 Ma to ~35 Ma) of zircons from different facies within the Coxacatlán pluton and observed mutual intrusion relationships documented between the mafic and grandiorite facies confirm that newer pulses were emplaced in an interval of ~4 m.y., without complete crystallization of previous pulses.

The clear time-space relationship between the Coxcatlán pluton intrusion, the uplift in the Coxcatlán-Tilzapotla dome area, and the Tilzapotla caldera formation strongly suggest that these episodes are part of a continuous magmatic development driven and thermally sustained by mafic magma recharge. U-Pb zircon ages that span approximately 6 m.y., starting at ~39 Ma in the west part of the dome (Coxcatlán pluton) to ~33 Ma in the east (Tilzapotla and Atopula ignimbrites and Chautle pluton), as well as the compositional variations of pluton facies and volcanic units in the area can be taken as evidence that the dome uplift was the result of gradual construction of a batholith underneath due to the injection of different magma batches.

What triggered the formation of the Tilzapotla caldera?

The last decade has seen major developments in understanding of causes of intense episodes of explosive silicic volcanism, or ignimbrite flare-ups. Large storage regions of eruptible magma are characterized as crystal mushes that may contain over 50% of crystals and may themselves erupt or may be the source of residual liquids that are extracted and then erupted (Lindsay *et al.*, 2001; Bachmann and Bergantz, 2008). According to numerical simulations of heat transfer in the upper crust, de Silva and Gosnold (2007) have shown that an elevated thermal flux is critical for the rheological conditions necessary to allow a large magma chamber to grow without erupting. These same conditions are necessary to maintain large melt-rich volumes of magma to feed caldera-forming eruptions (Annen, 2009). The recognition that such fluxes are most commonly found during magmatic flare-ups and are characteristic of batholith formation as well (*e.g.,* Ducea, 2001) suggests that a view where caldera forming eruptions and pluton formation require separate conditions is unwarranted. Large catastrophic caldera-forming eruptions that produce large ignimbrites are thus intimately associated with intrusive activity at depth (*e.g.*, Smith, 1979; de Silva *et al.*, 2006; Bachmann *et al.*, 2007b; Lipman, 2007). Extended plutonic activity would result in the development of crystal mushes that can lead to the accumulation of enough residual magma to produce a voluminous volcanic eruption. In such a scenario, the growing "batholith" reaches a point where the "domed" roof is extended, faulted, and mechanically unstable. At a "tipping point", the roof can be induced to collapse into the "chamber" producing a catastrophic caldera collapse (Gregg *et al.*, 2012) where most of the erupting crystal-mush accumulates as intra-caldera tuff (de Silva *et al.*, 2006). The relative abundance of phenocrysts in juvenile pumice fragments as well as the occurrence of glomerocrysts with abundant plagioclase in the Tilzapotla ignimbrite suggest that the major volcanic eruptions related to caldera formation were associated with the disruption of crystal mushes. Compared to the plutonic units, the narrower age range of zircons in population density plots of the Tilzapotla ignimbrite (Figure 7f, 7g) might be an indication of rapid development of the

eruptible magma in the central-eastern sector of the dome as the thermal conditions evolved (Figure 8). Overlapping zircon age ranges of the Tilzapotla ignimbrite and the small mafic Chautle pluton located near the caldera ring, as well as the Ar-Ar mineral age obtained for the Chautle pluton, which is within uncertainty of the zircon age, may suggest that injection of less evolved high-temperature magmas were instrumental in destabilizing crystal mushes (*e.g.*, Bachmann *et al.*, 2007b) and the roof and triggering caldera formation (Gregg *et al.*, 2012).

CONCLUSIONS

Zircon U-Pb dating of late Eocene plutons and ignimbrites of the Tilzapotla caldera indicates that they represent the record a long-lived magmatic system genetically related to the construction of the large scale Coxcatlán-Tilzapotla volcano-plutonic complex and associated structural dome. As suggested by compositional variations and the multiple injections recognized in the Coxcatlán pluton, the dome is the superficial expression of a batholith that progressively grew from a series of injections of silicic magmas into the upper crust. $^{40}Ar/^{39}Ar$ mineral cooling ages obtained for the Coxcatlán pluton are generally concordant with the weighted mean $^{206}Pb/^{238}U$ zircon ages, suggesting shallow emplacement and relatively rapid crystallization. U-Pb age ranges, as well as mean ages of the Coxcatlán pluton with respect to ignimbrites of the Tilzapotla caldera and the Buenavista and Chautle plutons, indicate a southeastward migration of the thermal anomaly with the highest intensity being underneath where the caldera developed. In the southeastern part of the dome, catastrophic caldera collapse occurred due to the magmatic system reaching a mechanical threshold where the extended and domed roof above the growing batholith was unstable and eventually failed. Recharge with less differentiated high-temperature magma may have been the trigger for the eruption and caldera (roof) collapse as it disrupted crystal mushes and destabilized the magma chamber.

APPENDIX A. SUPPLEMENTARY MATERIAL

Appendices A1 to A4 can be found at the journal web site <http://rmcg.unam.mx/>, in the table of contents of this issue.

ACKNOWLEDGEMENTS

Financial support for this study was provided by PAPIIT grant IN108210 and the Instituto de Geología, Universidad Nacional Autónoma de México. We would like to thank Cathy Busby and Allen F. Glazner for their careful reviews and valuable comments, which were helpful in improving the paper. S de Silva acknowledges support from the National Science Foundation to work on volcano-plutonic systems. We are grateful to Carlos Ortega-Obregón for assistance with the U-Pb zircon analyses, Rufino Lozano SantaCruz for the XRF analyses, Teresa Pi Puig for X ray diffraction analyses and, for the ^{40}Ar-^{39}Ar experiments, M.A. García Gracía for mass spectrometry, and A.S. Rosas Montoya, V.M. Pérez Arroyo and G. Rendon Márquez for sample preparation and evaluation.

REFERENCES

Andersen, T., 2002, Correction of common lead in U-Pb analyses that do not report ^{204}Pb: Chemical Geology, 192(1), 59-79.

Annen, C., 2009, From plutons to magma chambers: Thermal constraints on the accumulation of eruptible silicic magma in the upper crust: Earth and Planetary Science Letters, 284, 409-416.

Bachmann, O., Bergantz, G.W., 2008, Rhyolites and their source mushes across tectonic settings: Journal of Petrology, 49(12), 2277-2285.

Bachmann, O., Charlier, B.L.A., Lowenstern, J.B., 2007a, Zircon crystallization and recycling in the magma chamber of the rhyolitic Kos Plateau Tuff (Aegean Arc): Geology, 35, 73–76.

Bachman, O., Miller, C.F., de Silva, S.L., 2007b, The volcanic-plutonic connection as a stage for understanding crustal magmatism: Journal of Volcanology and Geothermal Research, 167, 1-23.

Bachmann, O., Oberli, F., Dungan, M.A., Meier, M., Mundil, R., Fischer, H., 2007c, $^{40}Ar/^{39}Ar$ and U-Pb dating of the Fish Canyon magmatic system, San Juan Volcanic field, Colorado: evidence for an extended crystallization history: Chemical Geology, 236, 134-166.

Barbarin, B., 1990, Plagioclase xenocrysts and mafic magmatic enclaves in some granitoids of the Sierra Nevada batholith, California: Journal of Geophysical Research, 95(B11), 17, 747-17, 756.

Carrizales-Aguilar, A., 1997, Informe de la visita de reconocimiento a los lotes mineros Cristo Rey, Arroyo y Arroyo 2, ubicados en el ejido Tlamacazapa municipio de Buenavista de Cuellar estado de Guerrero: Consejo de Recursos Minerales, Archivo Técnico 120374, 22 pp.

Coleman, D.S., Gray, W., Glazner, A.F., 2004, Rethinking the emplacement and evolution of zoned plutons: Geochronological evidence for incremental assembly of the Tuolumne Intrusive Suite, California: Geology, 32(5), 433-436.

de Cserna, Z., Fries, C., Jr., 1981, Hoja Taxco 14Q-h(7), con Resumen de la geología de la Hoja-Taxco, estados de Guerrero, México y Morelos: Universidad Nacional Autónoma de México, Instituto de Geología, Carta Geológica de México, 1:100 000 series, map with text.

de Silva, S.L., Gosnold, W.D., 2007, Episodic construction of batholiths: Insights from the spatiotemporal development of an ignimbrite flare-up: Journal of Volcanology and Geothermal Research, 167, 320-335.

de Silva, S., Zandt, G., Trumbull, R., Viramonte, J.G., Salas, G., Jiménez, N., 2006, Large ignimbrite eruptions and volcano-tectonic depressions in the Central Andes: a thermomechanical perspective: Geological Society, London, Special Publications, 269, 47-63.

Ducea, M., 2001, The California arc: Thick granitic batholiths, eclogitic residues, lithospheric-scale thrusting, and magmatic flare-ups: GSA Today, 11(11), 4-10.

Elías-Herrera, M., Sánchez-Zavala, J.L., Macías-Romo, C., 2000, Geological and geochronological data of Guerrero terrene in the Tejupilco area, southern Mexico: New constraints on its tectonic interpretation: Journal of South American Earth Sciences, 13, 355-375.

Elston, W.E., 1984, Mid-Tertiary ash-flow tuff cauldrons, southwestern New Mexico: Journal of Geophysical Research, 89, 8733-8750.

Ferrari, L., Orozco-Esquivel, T., Manea, V., Manea, M., 2012, The dynamic history of the Trans-Mexican Volcanic Belt and the Mexico

subduction zone: Tectonophysics, 522-523, 122-149.

Folkes, C.B., de Silva, S.L., Schmitt, A.K., Cas, R.A.F., 2011, A reconnaissance of U-Pb zircon ages in the Cerro Galán system, NW Argentina: Prolonged magma residence, crystal recycling, and crustal assimilation: Journal of Volcanology and Geothermal Research, 206, 136-147.

Fries, C., Jr., 1960, Geología del Estado de Morelos y de partes adyacentes de México y Guerrero, región central meridional de México: Universidad Nacional Autónoma de México, Instituto de Geología, Boletín 60, 229 pp.

Fries, C., Jr., 1966, Hoja Cuernavaca 14Q-h(8), Geología de la hoja Cuernavaca, Estado de Morelos: México, D.F., Universidad Nacional Autónoma de México, Instituto de Geología, Carta geológica de México, serie 1:100,00, map with text.

Glazner, A.F., Bartley, J.M., Coleman, D.S., Gray, W., Taylor, R.Z., 2004, Are plutons assembled over millions of years by amalgamation from small magma chambers?: GSA Today, 14(4-5), 4-11.

Gregg, P.M., de Silva, S.L., Grosfils, E.B., Parmigiani, J.P., 2012, Catastrophic caldera-forming eruption: Thermomechanics and implications for eruption triggering and maximum caldera dimensions on Earth: Journal of Volcanology and Geothermal Research, 241-242, 1-12.

Hora, J.M., Singer, B.S., Jicha, B.R., Beard, B.L., Johnson, C.M., de Silva, S., Salisbury, M., 2010, Volcanic biotite-sanidine $^{40}Ar/^{39}Ar$ age discordances reflect Ar partitioning and pre-eruption closure in biotite: Geology, 38(10), 923–926.

Kuiper, K.F., Deino, A., Hilgen, F.J., Krijgsman, W., Renne, P.R., Wijbrans, J.R., 2008, Synchronizing rock clocks of earth history: Science, 320(5875), 500-504.

Lindsay, J.M., Schmitt, A.K., Trumbull, R.B., de Silva, S.L., Siebel, W., Emmermann, R., 2001, Magmatic evolution of the La Pacana caldera system, Central Andes, Chile: Compositional variations of the cogenetic, large-volume felsic ignimbrite: Journal of Petrology, 42(3), 459-486.

Lipman, P.W., 1984, The roots of ash-flow calderas in western North America: Windows into the tops of granitic batholiths: Journal of Geophysical Research, 89, 8801–8841.

Lipman, P.W., 2007, Incremental assembly and prolonged consolidation of Cordilleran magma chambers: Evidence from the Southern Rocky Mountain volcanic field: Geosphere, 3(1), 42-70.

Lozano, R., Bernal, J.P., 2005, Characterization of a new set of eight geochemical reference materials for XRF major and trace element analysis: Revista Mexicana de Ciencias Geológicas, 22(3), 329-344.

Ludwig, K.R., 2008, Isoplot 3.70. A geochronological toolkit for Microsoft Excel: Berkeley Geochronology Center, Special Publications, 4, rev. August 26, 1-77.

Marshall, D.J., 1988, Cathodolunimescence of geological materials: Boston, Sydney, Wellington, Unwin Hyman, 146 pp.

Matzel, J.E.P., Bowring, S.A., Miller, R.B., 2006, Time scales of pluton construction at differing crustal levels: Examples from the Mount Stuart and Tenpeak intrusions, North Cascades, Washington: Geological Society of America Bulletin, 118 (11-12), 1412-1430.

McNulty, B.A., Tong, W., Tobisch, O.T., 1996, Assembly of a dike-fed magma chamber: The Jackass Lakes pluton, central Sierra Nevada, California: Geological Society of America Bulletin, 108(8), 926-940.

McNulty, B.A., Tobisch, O.T., Cruden, A.R., Gilder, S., 2000, Multistage emplacement of the Mount Givens pluton, central Sierra Nevada batholith, California: Geological Society of America Bulletin, 112(1), 119-135.

Meza-Figueroa, D., Valencia-Moreno, M., Valencia, V.A., Ochoa-Landín, L., Pérez-Segura E., Díaz-Salgado, C., 2003, Major and trace element geochemistry and $^{40}Ar/^{39}Ar$ geochronology of Laramide plutonic rocks associated with gold-bearing Fe skarn deposits in Guerrero state, southern Mexico: Journal of South American Earth Sciences, 16, 205-217.

Miller, J.S., 2008, Assembling a pluton…one increment at a time: Geology, 36(6), 511-512.

Miller, J.S., Matzel, J.E.P., Miller, C.F., Burgess, S.D., Miller, R.B., 2007, Zircon growth and recycling during the assembly of large, composite arc plutons: Journal of Volcanology and Geothermal Research, 167, 282-299.

Morán-Zenteno, D.J., Tolson, G., Martínez-Serrano, R.G., Martiny, B., Schaaf, P., Silva-Romo, G., Macías-Romo, C., Alba-Aldave, L., Hernández-Bernal, M.S., Solís-Pichardo, G.N., 1999, Tertiary arc-magmatism of the Sierra Madre del Sur, Mexico, and its transition to the volcanic activity of the Trans-Mexican Volcanic Belt: Journal of South American Earth Sciences, 12(6), 513-535.

Morán-Zenteno, D.J., Alba-Aldave, L.A., Solé, J., Iriondo, A., 2004, A major resurgent caldera in southern Mexico: the source of the late Eocene Tilzapotla ignimbrite: Journal of Volcanology and Geothermal Research, 136, 97-119.

Morán-Zenteno, D.J., Monter-Ramírez, A., Centeno-García, E., Alba-Aldave, L.A., Solé, J., 2007, Stratigraphy of the Balsas Group in the Amacuzac area, southern Mexico: relationship with Eocene volcanism and deformation of the Tilzapotla-Taxco sector: Revista Mexicana de Ciencias Geológicas, 24(1), 68-80.

Mori, L., Morán-Zenteno, D.J., Martiny, B.M., González-Torres, E.A., Chapela-Lara, M., Díaz-Bravo, B.A., Roberge, J., 2012, Thermomechanical maturation of the continental crust and its effects on the late Eocene-early Oligocene volcanic record of the Sierra Madre del Sur Province, southern Mexico: International Geology Review, 54(13), 1475-1496.

Ontiveros-Tarango, G., 1973, Estudio estratigráfico de la porción noroccidental de la Cuenca Morelos-Guerrero: Boletín de la Asociación Mexicana de Geólogos Petroleros, 25(4-6), 190-234.

Reid, M.R., 2003, Timescales of magma transfer and storage in the crust, *in* Rudnick, R.L., (ed.), Treatise on Geochemistry: Amsterdam, Elsevier, 263-292.

Sambridge, M.S., Compston, W., 1994, Mixture modeling of multi-component data sets with application to ion-probe zircon ages: Earth and Planetary Science Letters, 128, 373-390.

Schaaf, P., Morán-Zenteno, D., Hernández-Bernal, M. S., Solís-Pichardo, G., Tolson, G., Köhler, H., 1995, Paleogene continental margin truncation in southwestern Mexico: Geochronological evidence: Tectonics, 14(5), 1339-1350.

Schmitt, A.K., Grove, M., Harrison, T.M., Lovera, O., Hulen, J., Walters, M., 2003, The Geysers-Cobb Mountain magma system, California (Part 2): Timescales of pluton emplacement and implications for its thermal history: Geochimica et Cosmochimica Acta, 67(18), 3443-3458.

Sláma, J., Košler, J., Condon, D.J., Crowley, J.L., Gerdes, A., Hanchar, J.M., Horstwood, M.S.A., Morris, G.A., Nasdala, L., Norberg, N., Schaltegger, U., Schoene, B., Tubrett, M.N., Whitehouse, M.J., 2008, Plešovice zircon –A new natural reference material for U-Pb and Hf isotopic microanalysis: Chemical Geology, 249, 1-35.

Smith, R.L., 1979, Ash-flow magmatism, *in* Chapin, C.E., Elston, W.E., (eds.), Ash-flow Tuffs: Geological Society of America Special Paper 180, 5-27.

Smith, R.L., Bailey, R.A., 1968, Resurgent cauldrons, *in* Coates, R.R., Hay, R.L., Anderson, C.A., (eds.), Studies in Volcanology: Geological Society of America Memoir 116, 613–662.

Solari, L.A., Tanner, M., 2011, UPb.age, a fast data reduction script for LA-ICP-MS U-Pb geochronology: Revista Mexicana de Ciencias Geológicas, 28(1), 83-91.

Solari, L.A., Gómez-Tuena, A., Bernal, J.P., Pérez-Arvizu, O., Tanner, M., 2010, U-Pb zircon geochronology with an integrated LA-ICP-MS microanalytical workstation: achievements in precision and accuracy: Geostandards and Geoanalytical Research, 34(1), 5-18.

Steiger, R.H., Jäger, E., 1977, Subcommission on geochronology: Convention on the use of decay constants in geo- and cosmochronology: Earth and Planetary Science Letters, 36, 359-362.

Streckeisen, A., 1976, To each plutonic rock its proper name: Earth-Science Reviews, 12, 1-33.

Talavera-Mendoza, O., Ruiz, J., Gehrels, G.E., Meza-Figueroa, D.M., Vega-Granillo, R., Campa-Uranga, M.F., 2005, U-Pb geochronology of the Acatlán Complex and implications for the Paleozoic paleogeography and tectonic evolution of southern Mexico: Earth

and Planetary Science Letters, 235, 682-699.

Talavera-Mendoza, O., Ruiz, J., Gehrels, G.E., Valencia, V.A., Centeno–García, E., 2007, Detrital zircon U/Pb geochronology of southern Guerrero and western Mixteca arc successions (southern Mexico): New insights for the tectonic evolution of southwestern North America during the late Mesozoic: Geological Society of America Bulletin, 119(9/10), 1052-1065.

Tappa, M.J., Coleman, D.S., Mills, R.D., Samperton, K.M., 2011, The plutonic record of a silicic ignimbrite from the Latir volcanic field, New Mexico: Geochemistry, Geophysics, Geosystems, 12, Q10011, doi;10.1029/2011GC003700.

Vernon, R.H., 1986, K-feldspar megacrysts in granites – Phenocrysts, not porphyroblasts: Earth Science Reviews, 23, 1-63.

Vernon, R.H., Etheridge, M.A., Wall, V.J., 1988, Shape and microstructure of microgranitoid enclaves: indicators of magma mingling and flow: Lithos, 22, 1-11.

York, D., Evensen, N.M., López-Martínez, M., De Basabe-Delgado, J., 2004, Unified equations for the slope, intercept, and standard errors of the best straight line: American Journal of Physics, 72(3), 367-375.

Zimmerer, M.J., McIntosh, W.C., 2012, An investigation of caldera-forming magma chambers using the timing of ignimbrite eruption and pluton emplacement at the Mt. Aetna caldera complex: Journal of Volcanology and Geothermal Research, 245-246, 128-148.

Manuscript received: June 6, 2012
Corrected manuscript received: May 31, 2013
Manuscript accepted: June 1, 2013